NUMERICAL STUDIES OF A FAST Z-PINCH

by

Michael Andrew Christie

Physics Department

Imperial College

London SW7

Thesis submitted for the degree of Doctor of Philosophy of the University of London, and for the Diploma of Imperial College

October 1982

Abstract

The formation of the fast z-pinch at Imperial College has been studied numerically using several computer programs. A one dimensional two temperature "startup" program was written to follow the preionising phase of the discharge. Using the program the radial variation of the ionisation fraction, electron and ion temperatures and the magnetic field were obtained as functions of time.

The results from the "startup" program were used as initial conditions for a one dimensional program which followed the collapse of a z-pinch using the two temperature magnetohydrodynamic equations. A modular programming approach was adopted and the Flux Corrected Transport technique of Boris and Book was used for the hydrodynamics. Classical transport coefficients were used and a variable heat flux limit on the electron heat flux was imposed. Particular attention was paid to the effect of the low density plasma behind the magnetic piston and a "wall current" model was derived. The inclusion of the low density plasma by means of the wall current model was shown to lead to good agreement with experimental results on the fast z-pinch at Imperial College. The effect of the wall current model was to remove the large bounce after compression found in a previous numerical simulation of pinch formation.

Finally, the effect of the wall current model on an $m = 0$ instability of a z-pinch was considered. It was shown that the effect of the wall current model is second order in the amplitude of the instability, and that for realistic configurations the effect of the wall current model on the growth of the instability is small.

CONTENTS

Abstract	2
Contents	3
List of symbols	6
Acknowledgements	7
Chapter 1 Introduction	8
1.1 Introduction	8
1.2 Magnetohydrodynamics	11
1.3 Z-pinches	14
1.4 Analytic models of pinch formation	16
1.5 A Numerical model of pinch formation	22
Chapter 2 Preionising Stage of the z-pinch	29
2.1 Introduction	29
2.2 Preionising Circuit	30
2.3 Time dependent ionisation model	31
2.4 Numerical solution	35

2.4 Numerical solution 35

2.5 Results 41

2.6 Conclusions 45

Chapter 3 A simple wall current model 46

3.1 Introduction 46

3.2 Computational treatment of the vacuum region 47

3.3 A simple wall current model of the vacuum region 51

3.4 A simple computer program including the wall current model 55

3.5 Results from the model 62

3.6 Effect of varying γ 63

3.7 Conclusions 64

Chapter 4 Effect of wall currents on pinch formation 66

4.1 Introduction 66

4.2 MHD equations for pinch formation 68

4.3 Method of solution 75

4.4 Wall current model with resistive diffusion 79

4.5 Results 81

4.6 Conclusions 96

Chapter 5 Effect of wall currents on m = 0 instabilities 98

5.1 Introduction 98

5.2 A 2D FCT ideal MHD program 99

5.3 The long wavelength limit 102

5.4 Conclusions 109

Chapter 6 Conclusions 110

references 114

Appendix Monotonic conservative difference schemes 118

List of symbols

This list of symbols contains commonly used variables and those which are not defined where they first occur

ρ	density
$\underline{v}$	fluid velocity
t	time
p	pressure
γ	ratio of specific heats
$\underline{j}$	current density
$\underline{B}$	magnetic field
η	resistivity
I	current
r_p	piston position
r_s	shock position
θ_e	electron temperature (eV)
θ_i	ion temperature (eV)
τ_{eq}	equipartition time
n_e	electron number density
n_i	ion number density
Φ	magnetic flux
κ	thermal conductivity
μ	viscosity
L	inductance

With the exception of temperature, all units are MKS.

Acknowledgements

The work described in this thesis was carried out while I was a member of the Plasma Physics Group at Imperial College. I would like to thank my supervisor Prof M G Haines for his interest and encouragement during this work, and the Science Research Council for financial support.

I would also like to thank the other members of the Plasma Physics group with whom I have had many useful discussions; in particular I would like to thank Dr Deryck Bond for many useful discussions on theoretical plasma physics, and Peter Choi and Edmund Wyndham for giving me the experimentalist's view of the z-pinch.

CHAPTER 1

1.1 Introduction

The main theme of this thesis is the numerical simulation of a particular z-pinch experiment at Imperial College. The z-pinch experiment can be conveniently divided into three phases:

(1) the preionising phase

(2) the compression phase

(3) the confinement phase

The numerical simulation described in this thesis follows these phases, with the largest amount of work in stage (2) - the compression phase.

In chapter 2 the preionising phase of the z-pinch is examined. This stage is modelled with a two temperature model which ignores hydrodynamic effects. The working gas starts at room temperature with a seed ionisation fraction. The resistivity is determined by both electron-ion and electron-neutral collisions. As the preionising current is passed through the gas the electron and ions heat up until the gas becomes a fully ionised plasma at a temperature of about 10000 K. The results obtained are profiles of electron and ion temperatures, ionisation fraction, current density and magnetic field. These results are used to provide initial conditions for the programs which model the collapse phase of the pinch.

Chapter 3 considers the collapse phase of the formation of a z-pinch. The importance of the low density plasma in the "vacuum" region between the pinch boundary and the wall is discussed. The methods which have been used to treat this region in previous numerical simulations are described. All these methods treat the vacuum region as an insulator through which magnetic flux can diffuse infinitely quickly. While this leads to the correct behaviour during collapse, the subsequent expansion of the plasma is affected by the low density plasma. A model which treats the flux trapping in the low density plasma by means of wall currents is described, and a simple ideal MHD calculation is presented to show that the wall current model can have a significant effect on the pinch dynamics.

Chapter 4 presents a more detailed simulation of a real experiment. This experiment, on the fast z-pinch at Imperial College, had previously been modelled by Hopkins, Potter, and Webb (1978). They found good agreement between simulation and experiment at low filling pressures when viscous effects dominate during the final stages of the pinch. At higher filling pressures their results predicted a bounce out to 70% of the wall radius, whereas no significant bounce is observed experimentally. Rather than adapt their program, a new program, using the Flux Corrected Transport (FCT) technique of Boris and Book (1973) was written . The FCT program is written in modular form and can be run either as an Eulerian program or as a sliding rezone calculation. In the Eulerian calculation the low density plasma is modelled explicitly and diffusion of magnetic flux through

the wall after compression can be treated. In the sliding rezone calculation, the structure of the compressed pinch is resolved far more accurately than in the Eulerian calculation. Initially, the model used was the simple one described in Chapter 3 which does not treat the resistive diffusion of flux through the boundary; later a more advanced treatment was used which allowed for the diffusion of flux, and the sliding rezone calculation now provides as good treatment of the vacuum plasma and provides much better resolution of the pinch structure in space. Results presented include a comparison of the experimental trace of the piston position with the theoretical predictions for a run at high filling pressure. The experimental results show a steady outward movement of the piston which agrees well with the prediction, and which is due to the resistive decay of the wall current which prevents the large bounce.

Finally chapter 5 discusses the effect of the wall current model on the evolution of an m = 0 instability. Work by Book, Ott, and Lampe (1976) is extended to include the effect of wall currents. The effect is shown to be second order in the amplitude of the perturbation and therfore is nonlinear. By taking a favourable, but nonetheless realistic, case and showing that the effect is still small in the nonlinear stage of the instability, we can conclude that the wall current model cannot account for the anomalously long lifetime of the pinch observed experimentally by Choi et al (1978).

The rest of chapter 1 is organised as follows:
In section 1.2 we discuss the magnetohydrodynamic equations and the assumptions that lie behind them. The Bennett relation for an equilibrium z-pinch with a uniform temperature is derived because it is a fundamental relation in pinch theory. In section 1.3 we discuss pinches in general and give some simple calculations relating to a fusion z-pinch. The section is concluded with a discussion of the motivation behind the fast z-pinch experiment at Imperial College. In section 1.4 analytic models of pinch formation are reviewed - the widely known and widely used snowplough model, and the slug model of Potter. Section 1.5 concludes chapter 1 by reviewing the calculations of Hopkins, Potter and Webb (1978) on the formation of the z-pinch at Imperial College.

1.2 Magnetohydrodynamics

The magnetohydrodynamic equations are the equations of motion of an electrically conducting fluid. Because of their generality, they encompass a very wide range of physical phenomena, ranging from the study of electrical power generation from magnetohydrodynamic generators, through pinch devices and ionised flow around aircraft and missiles, to complex astrophysical phenomena such as solar flares, sunspots and the study of the magnetosphere. The magnetohydrodynamic equations can be written as

$$\frac{\partial \rho}{\partial t} + \nabla \cdot (\rho \underline{v}) = 0 \qquad (1.1)$$

$$\frac{\partial \rho \underline{v}}{\partial t} + \nabla \cdot (\rho \underline{v}\underline{v}) = -\nabla p + \underline{j} \times \underline{B} + \nabla \cdot \underline{\underline{\nu}} \qquad (1.2)$$

$$\frac{\partial p}{\partial t} + \nabla \cdot p\underline{v} = -(\gamma - 1) p \nabla \cdot \underline{v} + (\gamma - 1)\left\{ \eta j^2 + \mu (\nabla \cdot \underline{v})^2 \right\} \qquad (1.3)$$

$$\frac{\partial \underline{B}}{\partial t} = \nabla \times (\underline{v} \times \underline{B}) + \eta \nabla^2 \underline{B} \qquad (1.4)$$

$$\underline{j} = \nabla \times \underline{B} \qquad (1.5)$$

$$\nabla \cdot \underline{B} = 0 \qquad (1.6)$$

Eq (1.1) is called the continuity equation and represents conservation of mass. In eq(1.2), the momentum equation, the force on the plasma is given by the sum of the pressure gradient force and the Lorentz force $\underline{j} \times \underline{B}$. In the energy equation eq(1.3), the terms on the right hand side represent work done by the pressure and the effect of Joule heating. The induction equation eq(1.4) couples the magnetic field to the plasma. In the absence of resistivity ($\eta = 0$), the field lines

are "frozen-in" to the fluid. If the resistivity is nonzero, the magnetic field can slip through the fluid at a rate governed by the resistive diffusion time. Various assumptions have been made in deriving the magnetohydrodynamic equations. By neglecting space charge effects we have removed plasma oscillations from the system, and by neglecting the displacement current $\partial \underline{D}/\partial t$ we have made the assumption that all velocities are much smaller than the velocity of light.

Pressure balance and the Bennett relation

One of the fundamental results in pinch theory is the Bennett relation between the current, line density and the temperature in a pinch. A linear pinch is a long cylindrically symmetric system in which the radial pressure gradient $\partial p/\partial r$ is balanced by the $\underline{j} \times \underline{B}$ force. In the z-pinch the currrent is in the z direction and the magnetic field induced by the current is in the θ direction. If we now consider a z-pinch as shown in fig(1.1) and write the current $j = (0,0,j_z)$, and the magnetic field $B = (0,B(r),0)$ and the pressure $p = p(r)$, the equilibrium condition $\nabla p = \underline{j} \times \underline{B}$ can be written

$$\frac{\partial p}{\partial r} = \frac{B}{r}\frac{\partial}{\partial r}(rB) \tag{1.7}$$

Multiplying by r^2 and integrating out to the pinch radius a we find

$$-2\int_0^a rp\,dr = -\frac{1}{2\mu}\left(\frac{\mu_0 I}{2\pi}\right)^2 \tag{1.8}$$

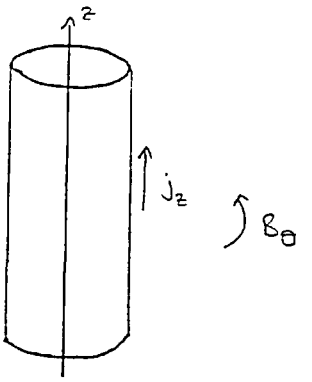


Fig 1.1 Schematic diagram of the pinch

where we have integrated by parts and used $P = \mu_0 I^2/2\pi a$ If we write $p = 2nkT$ and write the line rumber density

$$N = n\pi a^2$$

and make the assumption that the temperature is uniform across the pinch we obtain Bennett's relation

$$\mu_0 I^2 = 8\pi NkT \qquad (1.9)$$

1.3 Z-pinches

Much of the early work on pinch devices was done on the z-pinch and the θ-pinch because of their simplicity. Early calculations suggested that very high temperatures could be obtained in a pulsed linear discharge. For example, with a current of 0.5 MA and a line number density of 10^{17} cm^{-1}, the Bennett relation (eq 1.9) gives a plasma temperature of 16 keV. At this temperature and density the thermonuclear reaction rate would be very high (Artsimovitch,1964).

In a linear pinch the plasma is both confined and heated by its own magnetic field, and will make more efficient use of the energy input than toroidal devices since it will have a high average β ,i.e.

$$\langle \beta \rangle = \frac{\int p\,dr}{\int B^2/2\mu\,dr} \gtrsim 1$$

Unfortunately the simple z-pinch is highly unstable to the m = 0 and m = 1 (sausage and kink) instabilities. In early experiments these instabilities caused the plasma to hit the wall and resulted in a loss of confinement. Because of these problems and others such as end losses, research into controlled thermonuclear fusion concentrated on toroidal devices which can be stabilised to all MHD modes and which do not suffer from end losses.

There are two approaches to fusion experiments which can be characterised as magnetic containment and inertial containment. Their important characteristics are either low density and long containment time (magnetic confinement) or high density and short containment time (inertial confinement). The densities and confinement times for the different cases are shown below.

Inertial	$n \sim 10^{26}\ cm^{-3}$	10^{-12} s
Magnetic	$n \sim 10^{14}\ cm^{-3}$	1 s
z-pinch	$n \sim 10^{21}\ cm^{-3}$	10^{-7} s

In a toroidal device such as a Tokamak or a reversed field pinch in which the magnetic field is between 5 and 10 T the plasma density is limited to 10^{20} - 10^{21} m^{-3} by the requirement that $\beta < 1$. From the Lawson criterion this requires a containment time of several seconds for breakeven; furthermore consideration of the diffusion processes involved leads to a plasma radius of about 1 m (Haines,1981).

Until recently z-pinch experiments were limited by the low energies available from conventional capacitor banks. These limitations can now be overcome by using modern Blumlein technology (Choi,1978). Haines (1978) has considered the scaling of the z-pinch to fusion conditions, and has shown that by running at much higher input powers the z-pinch enters a new regime in which the Larmor radius is a sizeable fraction of the pinch radius. Thus substantial Finite Larmor Radius (FLR) stabilisation of unstable modes could occur. The fast z-pinch experiment at Imperial College is designed to use the Blumlein transmission line technology to investigate this regime.

1.4 Analytic models of pinch formation

The simplest model of pinch formation is the snowplough model. This is a skin current model in which the plasma pressure is neglected in comparison with the magnetic pressure. Assuming all the mass accretes at the pinch boundary we can write the equation of motion as

$$\frac{d}{dt}\left(\pi(r_b^2 - r_a^2)\rho_0 \frac{dr_b}{dt}\right) = 2\pi r_b \frac{B^2}{2\mu_0} \qquad (1.10)$$

Assuming a linear current rise $I(t) = \dot{I}t$ with $\dot{I}$ constant we have

$$\frac{d}{dt}\left\{(r_0^2 - r_p^2)\rho_0 \frac{dr_p}{dt}\right\} = -\frac{\mu_0 \dot{I}^2}{4\pi^2}\frac{t^2}{r_p} \qquad (1.11)$$

If we write $x = r_p/r_0$ and $\tau = t/t_0$ where

$$t_0^4 = 4\pi^2 \rho_0 / \mu_0 \dot{I}^2$$

we obtain the equation of motion of the pinch boundary given by the snowplough model

$$\frac{d}{d\tau}\left\{(1-x^2)\frac{dx}{d\tau}\right\} = -\tau^2/x \qquad (1.12)$$

The initial conditions are

$$x(0) = 1$$

$$\dot{x}(0) = 0$$

The slug model of pinch formation

Although the snowplough model is a simple and widely used model of pinch formation it has the disadvantage that it describes no structure in space. Potter (1978) has published a "slug" model of pinch formation which describes the radial structure of the pinch. The slug model predicts the formation of an equilibrium pinch whose radius is independent of the driving voltage or pinch current and depends only on the value of α and the wall radius.

Unfortunately the conclusion that an equilibrium pinch is formed appears to be incorrect. Nevertheless, the slug model is still a useful and interesting model of pinch formation. In the rest of this section the model is examined in some detail and is shown to predict a bounce after compression in the same way that the snowplough model does. This bounce makes it unnecessary to invoke an energy loss mechanism of outwardly travelling sound waves to explain conservation of energy.

Mathematical description of the slug model

Fig (1.2) shows the model taken for the formation of the pinch. A slug of plasma bounded by a shock at $r_s(t)$ and the magnetic piston at $r_p(t) > r_s(t)$ has a uniform pressure between shock and piston. The unshocked material has density ρ_0. The speed of the shock is $v_s = dr_s/dt$

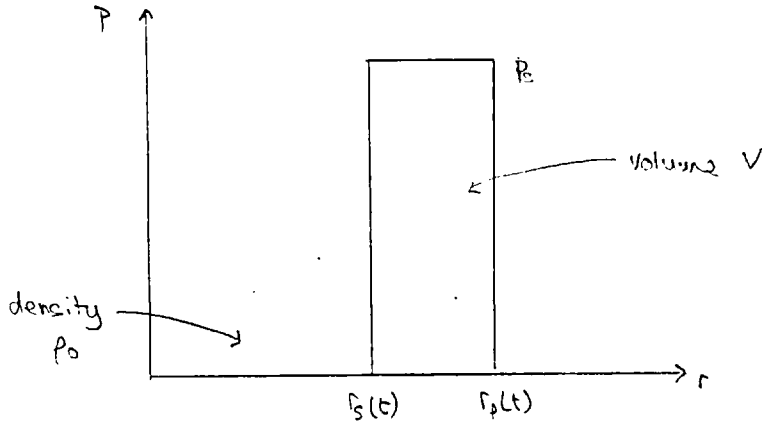


Fig 1.2 Finite region of compressed plasma in the slug model

By assuming that the shock thickness is small compared with finite r (an assumption which breaks down as the shock approaches the axis) the

Rankine - Hugoniot jump conditions can be applied to a shock in cylindrical geometry. Thus we obtain

$$u_s = \frac{2}{\gamma+1} v_s \tag{1.13}$$

$$\rho_s = \frac{\gamma+1}{\gamma-1} \rho_0 \tag{1.14}$$

$$p_s = \frac{2}{\gamma+1} \rho_0 v_s^2 \tag{1.15}$$

Between the shock and the piston the adiabatic law holds and so

$$\gamma p dV + V dp = 0 \tag{1.16}$$

From (1.15)

$$dp = \frac{2 dv_s}{v_s} p \tag{1.17}$$

The compressed plasma volume is given by

$$V = \pi (r_p^2 - r_s^2)$$

Using (1.13) we obtain

$$dV = 2\pi \left(r_p dr_p - \frac{2 r_s}{\gamma+1} dr_s \right) \tag{1.18}$$

Substituting this in (1.16) we obtain

$$r_p dr_p - \frac{2 r_s dr_s}{\gamma+1} + \frac{1}{\gamma}\left(r_p^2 - r_s^2\right)\frac{dv_s}{v_s} = 0 \qquad (1.19)$$

The other relation for the slug model comes from equating the magnetic pressure and the plasma pressure giving

$$v_s = \left(\frac{\mu_0}{\rho}\right)^{\frac{1}{2}} (\gamma+1)^{\frac{1}{2}} \; I/4\pi r_p \qquad (1.20)$$

If we combine (1.19) with (1.20) under the assumption of constant current we can obtain a relation between piston and shock radius

$$\left\{\frac{\gamma-1}{\gamma} + \frac{1}{\gamma}\frac{r_s^2}{r_p^2}\right\} dr_p = \frac{2}{\gamma+1}\frac{r_s}{r_p}\, dr_s \qquad (1.21)$$

This equation can be solved to give

$$r_p = r_0 \left(\frac{\gamma}{\gamma+1 - r_s^2/r_p^2}\right)^{\gamma/\gamma-1} \qquad (1.22)$$

which when $r_s = 0$ gives the pinch radius

$$a = r_0 \left(\frac{\gamma}{\gamma+1}\right)^{\gamma/\gamma-1} \qquad (1.23)$$

Potter solved eqs (1.19) and (1.20) numerically to obtain r_p, r_s as functions of time, and his graph is shown in fig(1.3). From his graph the plasma comes to rest when the shock hits the axis.

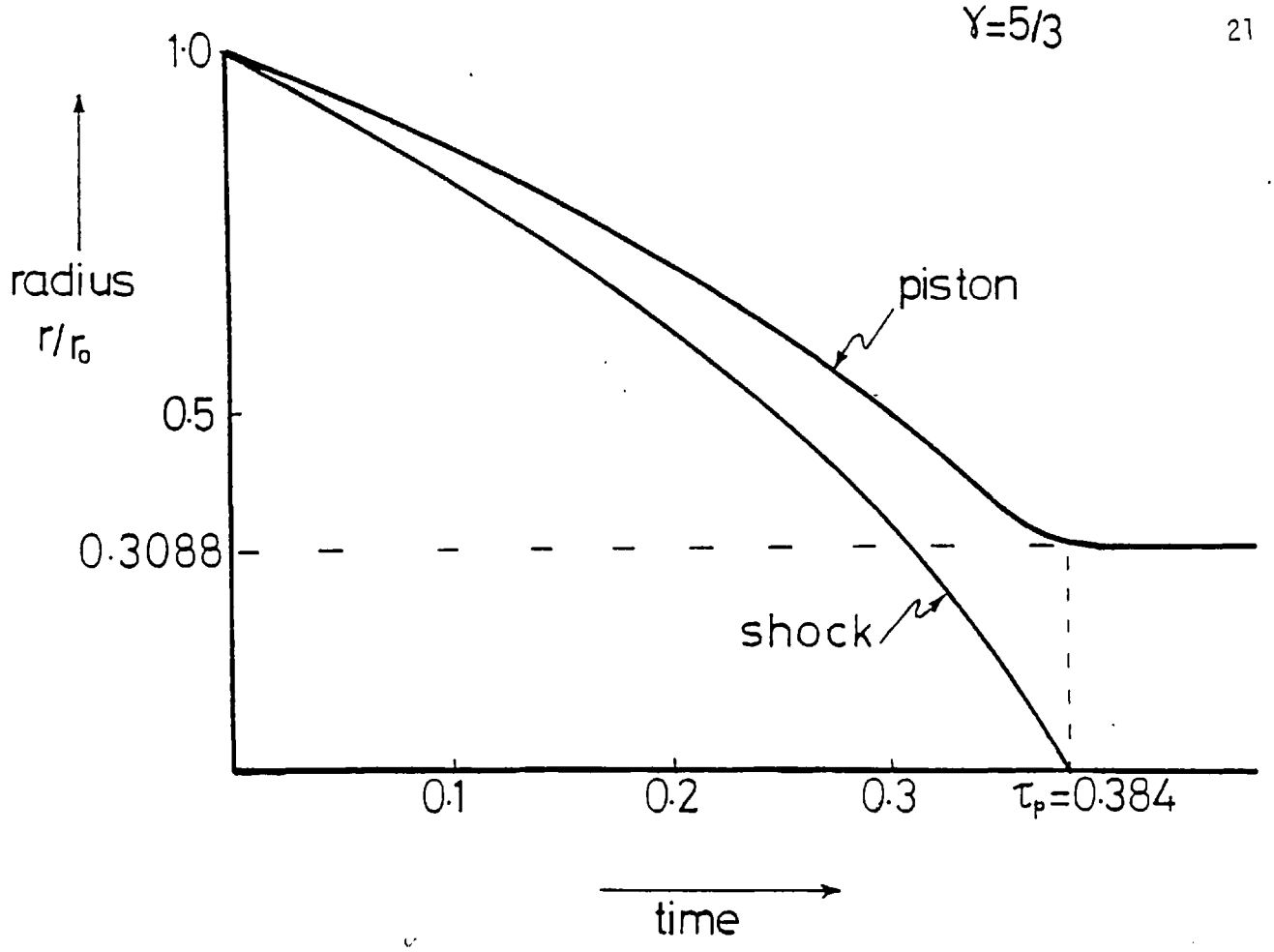


Fig 1.3 Dimensionless radius vs dimensionless time for the slug model

The conclusion that the plasma comes uniformly to rest and therefore remains at rest cannot be substantiated. This can be seen by evaluating the second derivative d^2r_s/dt^2 at $r_s = 0$. We find

$$\left.\frac{d^2r_p}{dt^2}\right|_{r_s=0} = \frac{2\gamma}{\gamma^2-1}\,\frac{v_s^2}{r_p} \qquad (1.24)$$

As t approches t_p (the time to pinch) d^2r_p/dt^2 is a constant for sufficiently small $|t - t_p|$. We must consider what happens to the shock as it hits the axis. From eq(1.20) we know that v_s^2 =const, and so we can just change the sign of v_s at $t = t_p$. This does not alter d^2r_p/dt^2 and so we obtain the equation for the pinch boundary close to the pinch time t .

$$r_p(t) = a + \frac{\gamma}{\gamma^2-1}\,\frac{V_s^2}{a}\,(t-t_p)^2 \qquad (1.25)$$

Since the pinch no longer comes to rest it is not necessary to invoke an energy loss mechanism of outwardly travelling sound waves in order to satisfy conservation of energy. Eq (1.25) is only valid for a short time after t_p because the shock is travelling outwards, and the model equations are no longer valid.

A recent paper by van Dyke and Guttman (1982) contains a more general analysis of the problem of a converging shock wave. They expand all variables in a power series expansion in time in terms of polynomials in the distance from the piston. Initially (to second order in t/t_p) the pressure remains uniform between shock and piston, but at late times this does not hold. The examples they give refer to a collapse with constant piston speed, but their method could be used to investigate the formation of a z-pinch. Thus, we can conclude that the results predicted by the slug model close to the pinch time will be in error because the assumption of uniform pressure between shock and piston breaks down at late times.

1.5 A numerical model of pinch formation

Hopkins, Potter and Webb (1978) developed a one dimensional single fluid magnetohydrodynamic computer program to study the formation of the fast z-pinch at Imperial College. Rather than difference the magnetohydrodynamic equations as they stand, a novel method was

employed in which the model itself was discretised and exact equations from the model were solved. In the model the plasma is represented by a finite train of cells with uniform pressure in each cell. Current is allowed to flow only at cell boundaries. In the absence of diffusive effects mass, entropy and magnetic flux are conserved in each cell. This approach is analogous to the "waterbag" method.

Considering only the ideal magnetohydrodynamic equations at first (diffusive effects will be included later) and letting m_i be the mass in each cell, $\epsilon_i = p/\rho_i^{\gamma}$ and ϕ_i the magnetic flux, the MHD equations when integrated over each cell yield three conservation relations and an equation of motion

$$\frac{dm_i}{dt} = 0 \tag{1.26}$$

$$m_{i-\frac{1}{2}} \frac{dv_{i-\frac{1}{2}}}{dt} = \left(p_{i-1}^{TOT} - p_i^{TOT}\right)_{i-\frac{1}{2}} \tag{1.27}$$

$$\frac{d\epsilon_i}{dt} = 0 \tag{1.28}$$

$$\frac{d\phi_i}{dt} = 0 \tag{1.29}$$

where $P_i^{TOT} = p_i + B_i^2/2$

The magnetic field B in each cell i can be expressed as

$$B_i = I_{i-1/2}/r_i$$

where $I_{i-1/2}$ = the total current flowing in the region $(0, r_{i-1/2})$ and is related to the magnetic flux by

$$\phi_i = I_{i-1/2} \log\left(r_{i+1/2}/r_{i-1/2}\right) \tag{1.30}$$

The assumption that current only flows at cell boundaries means that the $\underline{B}.\nabla\underline{B}$ term is zero. To integrate the equation of motion eq(1.27), the hydrostatic and magnetic pressure terms are separated to give

$$m_{i-1/2}\frac{dv_{i-1/2}}{dt} = (p_{i-1}-p_i)r_{i-1/2} + \left(\frac{I_{i-3/2}^2}{2r_{i-1}^2} + \frac{I_{i-1/2}^2}{2r_i^2}\right)r_{i-1/2} \tag{1.31}$$

The right hand side must be expressed at the time n+½ and the following two identities (correct to $O(\Delta t^2, \Delta x^2)$ are needed

$$p_i^{n+1/2} r_{i-1/2}^{n+1/2} = \left(r_{i-1/2}^n p_i^n + r_{i-1/2}^{n+1} p_i^{n+1}\left(\frac{r_i^n}{r_i^{n+1}}\right)^\gamma\right)\left(1 - \frac{\gamma\Delta t}{4r_i^n}\left(v_i^n + v_i^{n+1}\right)\right) \tag{1.32}$$

and

$$\log\left(r_{i+1/2}^{n+1/2}/r_{i-1/2}^{n+1/2}\right) = \log\left(r_{i+1/2}^n/r_{i-1/2}^n\right) + \frac{\Delta t}{2r_{i+1/2}^n}v_{i+1/2}^{n+1/2} - \frac{\Delta t}{2r_{i-1/2}^n}v_{i-1/2}^{n+1/2} \tag{1.33}$$

for $\Delta t\, v_{i-1/2}^{n+1/2}/2r_{i-1/2}^n < 1$

The new cell boundary positions are given by

$$r_{i+1/2}^{n+1} - r_{i+1/2}^n = \Delta t\, v_{i+1/2}^{n+1/2}$$

and thus an iterative implicit scheme involving a tridiagonal matrix inversion is obtained for the solution of the cell boundary

velocities.

The procedure described above allows the computation of solutions for the formation of an ideal pinch. When transport terms are included conservation of entropy and magnetic flux no longer hold in each cell. Instead eqs (1.28),(1.29) are replaced by diffusion equations. The effect of viscosity is included by means of an extra viscous pressure in the momentum equation. In order to include the extra viscous pressure, Hopkins, Potter and Webb derived an expression for the force on a radial surface from viscous effects using the divergence theorem as follows. The viscous force on a volume is given by

$$\int \nabla \cdot \underline{\underline{T}} \, d\tau = \int_S \underline{\underline{T}} \cdot d\underline{S} \tag{1.34}$$

and therefore the radial force is given by the r component of $\underline{\underline{T}} \cdot d\underline{S}$. This expression was evaluated as

$$F_r^{visc} = \sigma_{rr} r \tag{1.35}$$

The correct expression is given by

$$F_r^{visc} = \sigma_{rr} r + \sigma_{r\theta} \tag{1.36}$$

Eq (1.35) when evaluated leads to a viscous pressure given by

$$\pi = -\mu \left(2 \frac{\partial v}{\partial r} + \frac{2}{r} v \right) \tag{1.37}$$

Eq(1.36) leads to the expression

$$\pi = -\frac{4}{3}\mu\nabla\underline{v} \qquad (1.38)$$

This latter expression can be seen to be the correct form by writing the Navier-Stokes viscous term (which is not $\mu\nabla^2\underline{v}$ since $\nabla.\underline{v}\neq 0$!) as (Batchelor, 1967),

$$\mu\,\nabla\times(\nabla\times\underline{v}) + \frac{4}{3}\nabla\mu\nabla\underline{v} \qquad (1.39)$$

which when $\nabla\times\underline{v}=0$ gives

$$\pi = -\frac{4}{3}\mu\nabla.\underline{v} \qquad (1.40)$$

Since this is a vector identity it is valid in any coordinate system in which $\nabla\times\underline{v}=0$. In particular it applies to radial motion in cylindrical coordinates. However it should be noted that the difference between the two expressions is negligible for most of the simulation and is only important for small r.

Including thermal conductivity and resistivity leads to diffusion equations for entropy and magnetic flux which are differenced fully implicitly to avoid inaccuracies when the timestep is much larger than the explicit timestep.

Two sets of results from this program are shown for comparison with the results presented later on. The first set of graphs (Fig 1.4) shows the solutions obtained for a 1cm radius z-pinch at a filling pressure of 80mTorr. At this filling pressure, viscous effects are

important as the pinch hits the axis, and no outward bounce is observed. In fig(1.5), results from a run at 300 mTorr filling pressure are shown. Here viscosity is much less important, and a large outward bounce is predicted. The experimental results do not show this bounce, and we will see later on that the low density plasma outside the pinch could be responsible for removing this bounce.

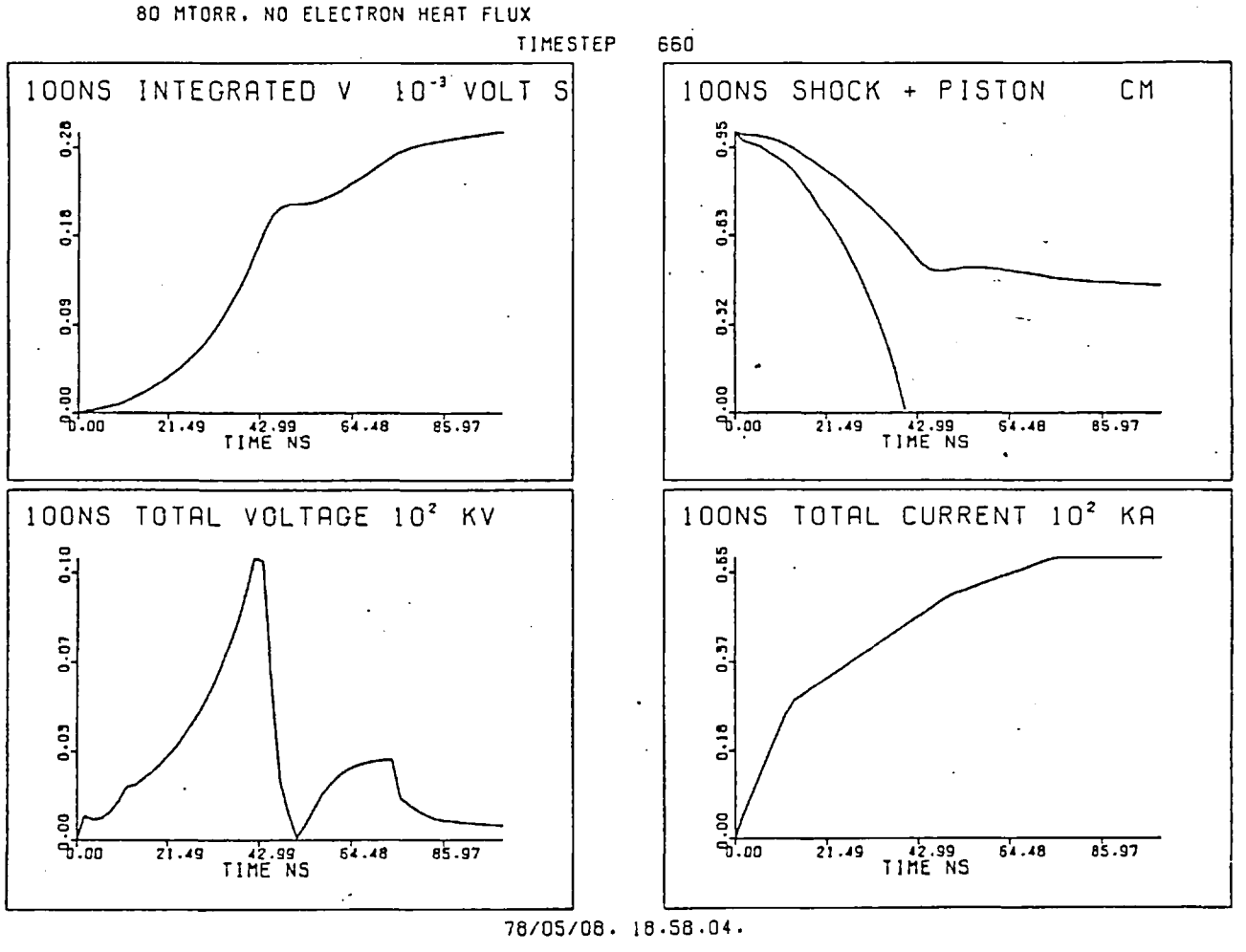


Fig 1.4 Solutions from the Hopkins, Potter, Webb model

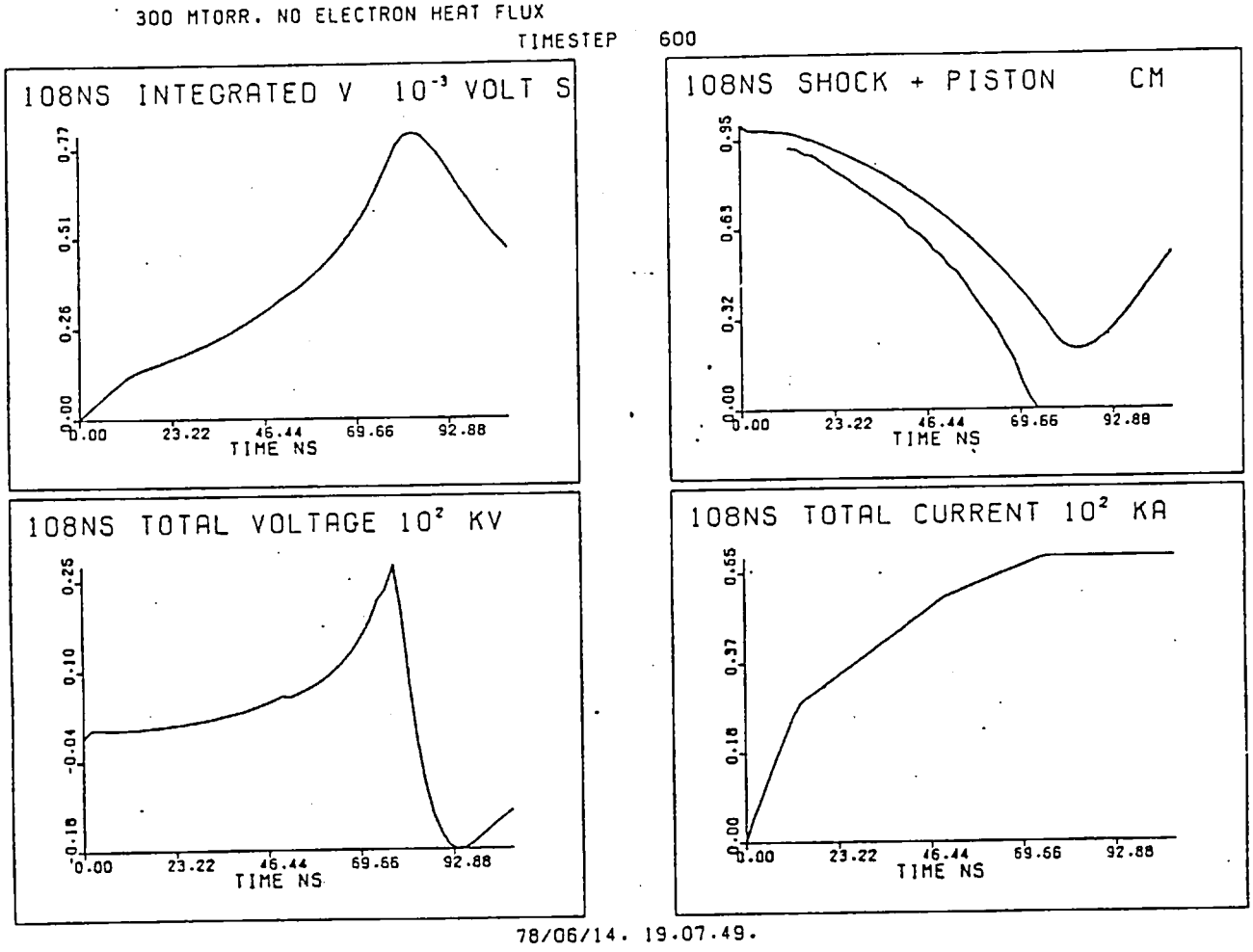


Fig 1.5 Solutions from the Hopkins, Potter, Webb model

CHAPTER 2

2.1 Introduction

In this chapter we describe the numerical simulation of the preionising phase of a z-pinch. The problem is highly nonlinear and must be solved numerically . From the numerical solutions obtained, the plasma state before the main discharge is known and the initial conditions for the program described in chapter 4 can be verified.

In a z-pinch the discharge vessel is initially filled with a low pressure gas at room temperature. The gas must be ionised before it becomes a plasma and this is accomplished by discharging a capacitor bank through the pinch. Initially the gas is almost entirely neutral and the resistivity is determined by electron neutral collisions. The gas is heated by Joule heating and this energy goes into heating the charged particles and ionising the neutrals. As the gas heats up the ionisation fraction increases and the resistivity changes over a wide range. The final result is a plasma at a temperature of one or two eV which is nearly fully ionised (the ionisation fraction varies from about 70% on axis to almost 100% at the wall).

We model the preionising phase of the z-pinch in cylindrical geometry. Neglecting thermal conduction and hydrodynamic motion we obtain a parabolic partial differential equation for magnetic field diffusion and a set of coupled ordinary differential equations at each point for

ionisation rate and for energy balance. With the exception of the change in geometry the equations used are those used by Killen, Gibson and Colgate (1960). The equation for magnetic field diffusion is linked to a simple circuit equation to reproduce the main features of the preionising circuit used in the experiment at Imperial College.

2.2 Preionising Circuit

In order to obtain results which agree with experimental observations we need to have some model for the circuit. For the fast z-pinch at Imperial College the equivalent preionising circuit is shown in fig(2.1).

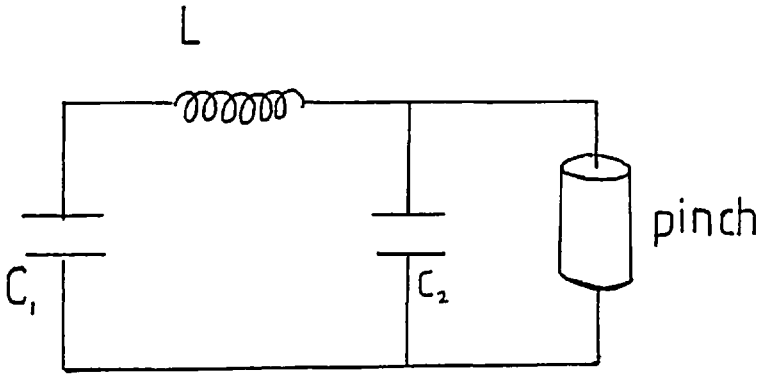


Fig 2.1 Equivalent preionising circuit

C_1 is charged to 60 kV, and L and C_2 are chosen so that the ringing frequency of the circuit formed by C_1, L, and C_2 is $\omega \simeq 1.5 \times 10^6 s^{-1}$.

In the STARTUP program, we model the circuit as shown below

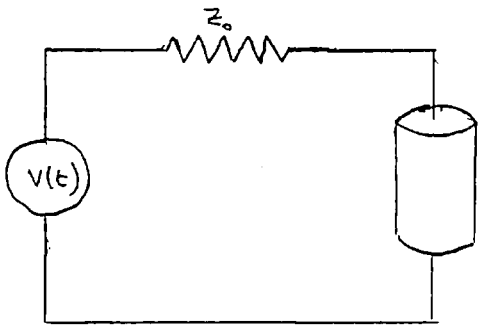


Fig 2.2 Model preionising circuit

where $V(t) = V_o \sin \omega t$

with $V_o = 60kV$ and $\omega = 1.57 \cdot 10^6 s^{-1}$

This is a valid approximation for most of the preionising phase when the impedance of the pinch is still very high. The value of Z_o is chosen so that the preionising current is roughly that observed experimentally (i.e. about 5kA), and the current through the pinch when the impedance is small still agrees with experiment.

2.3 Time dependent ionisation model

Killeen, Gibson and Colgate (1960) considered boundary layer formation in the pinch by studying magnetic field diffusion in cartesian geometry linked to equations for electron and ion temperature and ionisation fraction. We are interested in the behaviour of the plasma

properties across the whole pinch, and not just in a narrow boundary layer at the edge, and so we use the ordinary differential equations given by Killeen et al with magnetic field diffusion in cylindrical symmetry. These equations are used to follow the evolution of the plasma from a gas at room temperature to a fully ionised plasma at a temperature of one or two eV.

Plasma variables and model equations

The variables we use to describe the plasma are the electron and ion temperatures Θ_e, Θ_i (measured in eV), the ionisation fraction, f, given by the electron number density divided by the initial neutral number density, n_o, and the magnetic field B. The magnetic field is linked to the rest of the variables through the resistivity η which arises from both electron-ion and electron-neutral collisions.

In the equations used in this chapter the effects of thermal conduction and hydrodynamic motion are ignored. Neglecting hydrodynamic motion simplifies the problem enormously. It can be justified because for most of the preionising phase the hydrodynamic timescale is by far the longest. This assumption breaks down as the pinch becomes fully ionised. Neglecting thermal conduction can be justified by noting that for most of the ionisation phase the current and resistivity are uniform across the pinch and the joule heating does not introduce temperature gradients. Including thermal conduction would be a simple matter in cases where

it was necessary.

Assuming cylindrical symmetry and an infinitely long pinch, the equations to be solved are

$$\frac{\partial B}{\partial t} = \frac{\partial}{\partial r}\left(\frac{\eta}{\mu r}\frac{\partial}{\partial r} rB\right) \tag{2.1}$$

$$\frac{\partial \Theta_i}{\partial t} = \frac{\Theta_e - \Theta_i}{\tau_{eq}} \tag{2.2}$$

$$\eta j^2 = \epsilon_0 \frac{\partial n_e}{\partial t} + \frac{\partial}{\partial t}\left(\frac{3}{2} n_e e \Theta_e + \frac{3}{2} n_i e \Theta_i\right) \tag{2.3}$$

and

$$\frac{\partial n_e}{\partial t} = n_e (n_0 - n_e) \langle \sigma v \rangle \tag{2.4}$$

Equations (2.1) and (2.2) are straightforward and simply represent magnetic field diffusion and equipartition of energy from electrons to ions. Equation (2.3) is an energy equation in which joule heating gives rise to ionisation of neutrals and heating of charged particles. ϵ_0 is an average ionisation potential, and the term $\epsilon_0 \partial n_e/\partial t$ represents an energy loss from the electrons.

Equation (2.4) is the ionisation rate equation for ionisation by electron-neutral collisions, and the term $\langle \sigma v \rangle$ is obtained by averaging the cross section over a Maxwellian velocity distribution. The ionisation cross section is the one used by Killeen et al (1960). They used a fit to published experimental results (from Mott and

Massey, 1949), and obtained

$$\langle \sigma v \rangle = 2a_0^2 \sqrt{\frac{2\pi\theta_e}{m_e}} \left\{ \begin{array}{l} (1.8 + 4/3\alpha + 8/\alpha^2)e^{-\alpha} \\ \quad + (-.16 + .987/\alpha + .8/\alpha^2)e^{-4\alpha} \\ \quad\quad + (.8 + .08/\alpha)e^{-20\alpha} \end{array} \right\} \qquad (2.5)$$

where $\alpha = \epsilon_\omega/\theta_e$, and πa_0^2 is the atomic cross section. There is no recombination term in this equation. Recombination (which is proportional to f^3) will change the equilibrium ionisation fraction to a value less than 1.*

The two quantities remaining to be defined are the resistivity η and the equipartition term τ_{eq} . The resistivity is due to electron-ion and electron-neutral collisions, and is given by

$$\eta = \frac{m}{ne^2}(\nu_{ei} + \nu_{en}) \qquad (2.6)$$

where ν_{ei} and ν_{en} are the electron-ion and electron-neutral collision frequencies.

The equipartition time is given by

$$\tau_{eq} = \frac{m_i}{2m_e} \frac{1}{\nu_{ei}} \qquad (2.7)$$

and the two collision frequencies are given by (Miyamoto, 1980)

* This means that a Saha equilibrium cannot be reached, and the results may not be valid if recombination is important

$$\nu_{ei} = \frac{n_e Z e^4 \log\Lambda}{28.8\,\pi^{1/2}\,\epsilon_0^2\, m_e^{1/2}\, T_e^{3/2}} \qquad (2.8)$$

$$\nu_{en} = (n_0 - n_e)\sqrt{\frac{3e\theta_e}{m_e}}\;\sigma_{en} \qquad (2.9)$$

with $\sigma_{en} = 5.10^{-19}\ m^2$.

The choice of a constant collision frequency was criticised by Rose and Clarke (1965), and a graph of collision cross-section is shown in fig (2.3). In practice varying σ_{en} over a limited range made very little difference to the final state of the pinch.

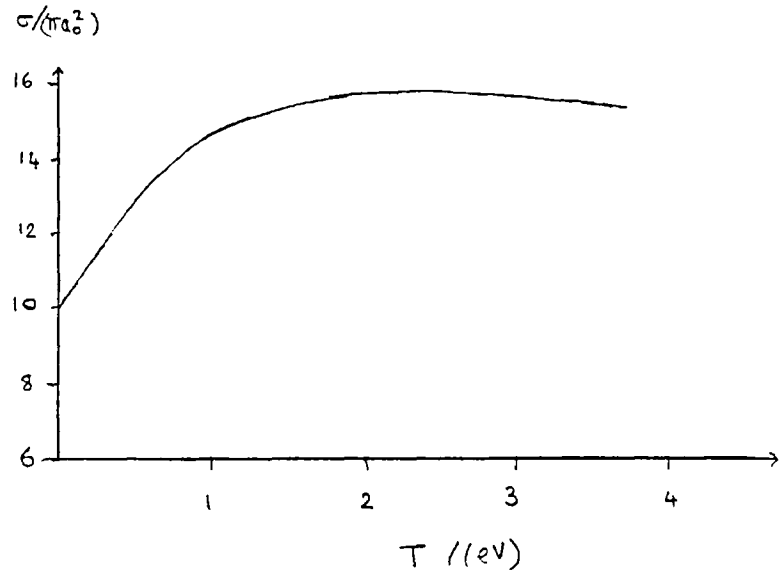


Fig 2.3 Normalised collision cross section vs temperature

2.4 Numerical solution

Writing the ionisation fraction $f = n_e/n_0$, the equations of the previous section are solved in the form

$$\frac{\partial B}{\partial t} = \frac{\partial}{\partial r}\left(\frac{\eta}{\mu_0 r}\frac{\partial}{\partial r}rB\right) \qquad (2.10)$$

$$\frac{\partial \theta_i}{\partial t} = (\theta_e - \theta_i)/\tau_{eq} \tag{2.11}$$

$$\frac{\partial \theta_e}{\partial t} = -\frac{\partial \theta_i}{\partial t} + \frac{2}{3f}\left(\frac{n_j^2}{n_{oe}} - \left(\epsilon_0 + \frac{3}{2}(\theta_e + \theta_i)\right)\frac{\partial f}{\partial t}\right) \tag{2.12}$$

$$\frac{\partial f}{\partial t} = f(1-f)\langle \sigma v \rangle \tag{2.13}$$

$$n_j = n_{ei} + n_{en} \tag{2.14}$$

$$n_{ei} = C_{ei} 2 \log \Lambda\, \theta_e^{-3/2} \tag{2.15}$$

$$n_{en} = C_{en}(1-f)\theta_e^{1/2}/f \tag{2.16}$$

$$\langle \sigma v \rangle = C_{\gamma sn}\, h(\theta_e/\epsilon_0) \tag{2.17}$$

where the form of the function h is given in eq. (2.5) and the coefficients C_{ei}, C_{en}, $C_{\gamma sn}$ are evaluated from eqs. (2.7), (2.8), and (2.9).

The magnetic field is defined at $r'_i = (i-1)\Delta r$, $i = 1, \ldots N+1$, and all other quantities are defined at $r_i = (i-\tfrac{1}{2})\Delta r$, $i = 1, \ldots N$. This choice allows satisfactory treatment of the boundary conditions and results in the current density being defined on the same grid as the electron and ion temperatures and the ionisation fraction.

Equations (2.11) - (2.13) are ordinary differential equations to be integrated forward in time at each mesh point of the simulation region. A fourth order Runge - Kutte integration routine is used to advance the equations forward in time.

The Runge - Kutte integration routine used is described by Fox and Mayers (1968) and is given by the following algorithm for an equation of the form

$$dy/dx = f(y, x)$$

$$k_1 = f(x_n, y_n)$$

$$k_2 = f(x_n + h/2, y_n + k_1 h/2)$$

$$k_3 = f(x_n + h/2, y_n + k_2 h/2)$$

$$k_4 = f(x_n + h, y_n + h k_3)$$

$$y_{n+1} = y_n + \frac{h}{6}(k_1 + 2k_2 + 2k_3 + k_4) + O(h^5)$$

where $h = x_{n+1} - x_n$ is the integration step.

The truncation error is given by

$$E_{n+3} = \{10y_n + 9y_{n+1} - 18y_{n+2} - y_{n+3} + 3h[f_n + 6f_{n+1} + 3f_{n+2}]\}/30$$

It would be possible to include an automatic timestep control based on this expression. This is not done in the program and instead the timestep is controlled in a more ad hoc fashion by requiring that the percentage change in any one variable is less than a specified maximum.

While the method described here is quite adequate for the problem solved, there are many more efficient integration methods for ordinary differential equations . If the ionisation calculations were included in a hydrodynamics program a stiff set of ordinary differential equations would result and a far more efficient solution method would be required. Two possible routines are Gear's algorithm (Gear, 1971), or the RIKM routine described by Howells and Marshall (1981). They use an implicit Runge - Kutte - Merson scheme with an automatic timestep controller based on an expression for the local truncation error similar to that given above. The RIKM scheme is able to use a timestep approaching the longest timescale of interest, and Howells and Marshall report about a 40% improvement in running time over explicit Runge - Kutte - Merson schemes.

Eq.(2.10) for magnetic field diffusion is differenced fully implicitly in time. The reason for this choice of method is that initially the resistive diffusion time τ_d is by far the shortest timescale and so a scheme which obtains the correct steady state solution to eq(2.10) is needed. Later on in the simulation τ_d is by far the longest timescale and the timestep chosen by the Runge - Kutte integrator is

small enough for the truncation error associated with a first order method to be neglected.

The boundary conditions on (2.10) are

$$B(0) = 0 \tag{2.18}$$

$$\eta j|_{wall} = E_{wall} \tag{2.19}$$

The voltage across the plasma is

$$V_{wall} = V(t) - I(t) Z_0$$

and therefore the electric field at the wall is given by

$$E_{wall} = \frac{V(t)}{L} - 2\pi r_{wall} B_{wall} Z_0 / \mu_0 L$$

If we difference eq.(2.10) fully implicitly we obtain

$$-\alpha_i B_{i-1}^{n+1} + \beta_i B_i^{n+1} - \gamma_i B_{i+1}^{n+1} = B_i^n \tag{2.20}$$

where

$$\gamma_i = \frac{\Delta t}{\Delta r^2} \frac{\eta_i r'_{i+1}}{\mu r_i} \tag{2.21}$$

$$\alpha_i = \frac{\Delta t}{\Delta r^2} \frac{\eta_{i-1} r'_{i-1}}{\mu r_{i-1}} \tag{2.22}$$

$$\beta_i = 1 + \alpha_i + \gamma_i \tag{2.23}$$

By substituting (2.20) into (2.19) and evaluating at time level n + 1, we can obtain the boundary condition at r_{wall} as

$$B_{N+1}^{n+1} = a + b\, B_N^{n+1} \tag{2.24}$$

where

$$a = V(t+\Delta t) \Big/ \left(\frac{n_N L l'_{N+1}}{\mu \Delta r} + \frac{2\pi r_w z}{\mu_0} \right) \tag{2.25}$$

$$b = n_N L l'_N \Big/ \left(n_N L l'_{N+1} + \Delta r 2\pi r_w z \right) \tag{2.26}$$

With the boundary condition at r = 0

$$B_0^{n+1} = 0 \tag{2.27}$$

eq(2.21) is a tridiagonal matrix equation which can be inverted by the usual algorithm (see eg Roache, 1972).

2.5 Results

In this section results from the STARTUP program are presented. The program was run to obtain the spatial variation of the plasma variables for a 1 cm radius z-pinch at filling pressures of 80 and 300 mTorr. The plasma column formed has roughly equal electron and ion temperatures and is fully ionised at the edge.

In fig 2.4 the radial variation of ionisation fraction for a filling pressure of 300 mTorr is shown at four times during the ionisation. The initial ionisation fraction was 10^{-6}. As the electric field is applied across the pinch, the most of the energy goes into heating the electrons. As the electron temperature rises to about 1eV, the resistivity decreases and the collisional ionisation rate increases. The electron temperature decreases as more electrons are ionised and the electron energy is shared among a larger number of particles.

At about 190 ns, the resistance of the pinch has dropped to a value at which the current is limited by the external impedance. This can be seen in fig 2.6 (where the voltage and current have been normalised to 1, and the time axis is scaled to the ionisation time). At this time the voltage across the pinch drops and the current through the pinch increases. The resistive diffusion time is still short enough for the magnetic field to diffuse through the pinch, but as the pinch heats up the resistive diffusion time increases and a boundary layer starts to form.

In fig 2.5 the plasma variables are plotted against the plasma radius

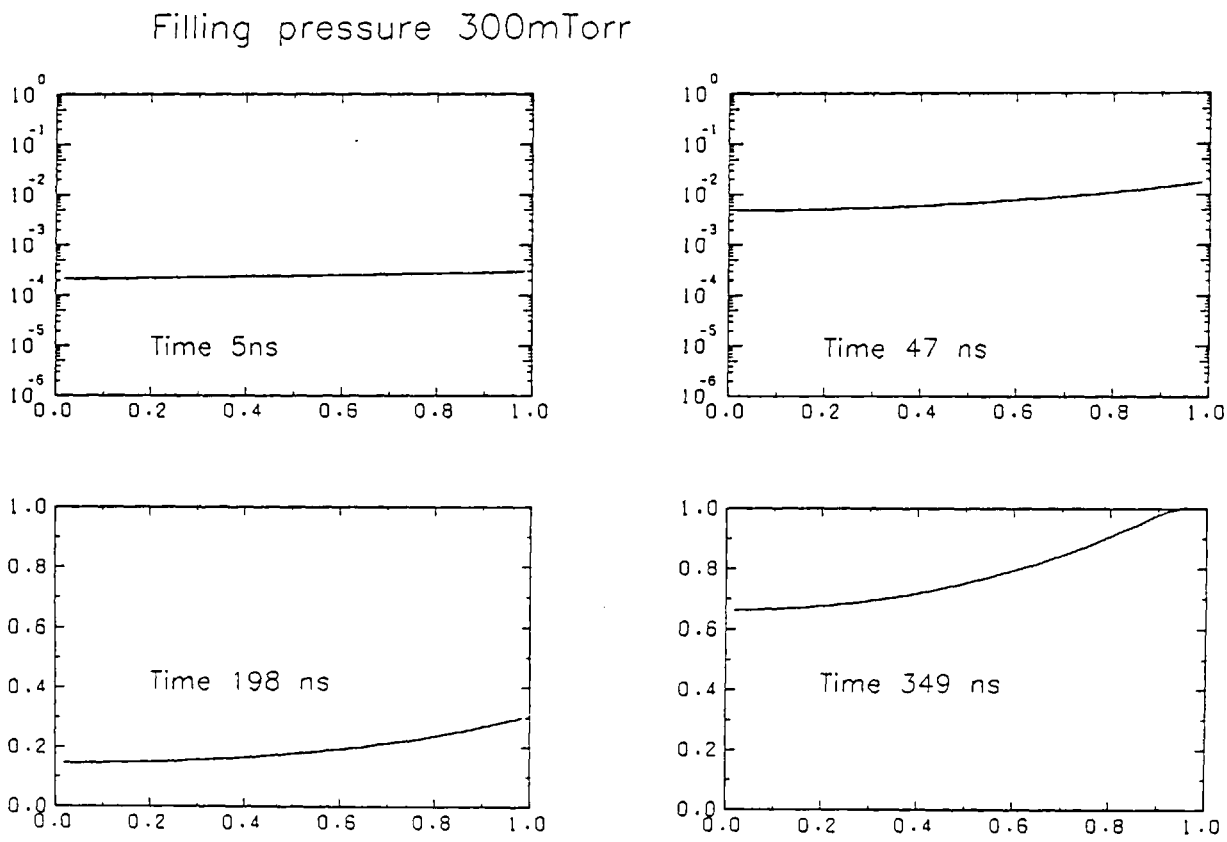


Figure 2.4

ionisation fraction against radius

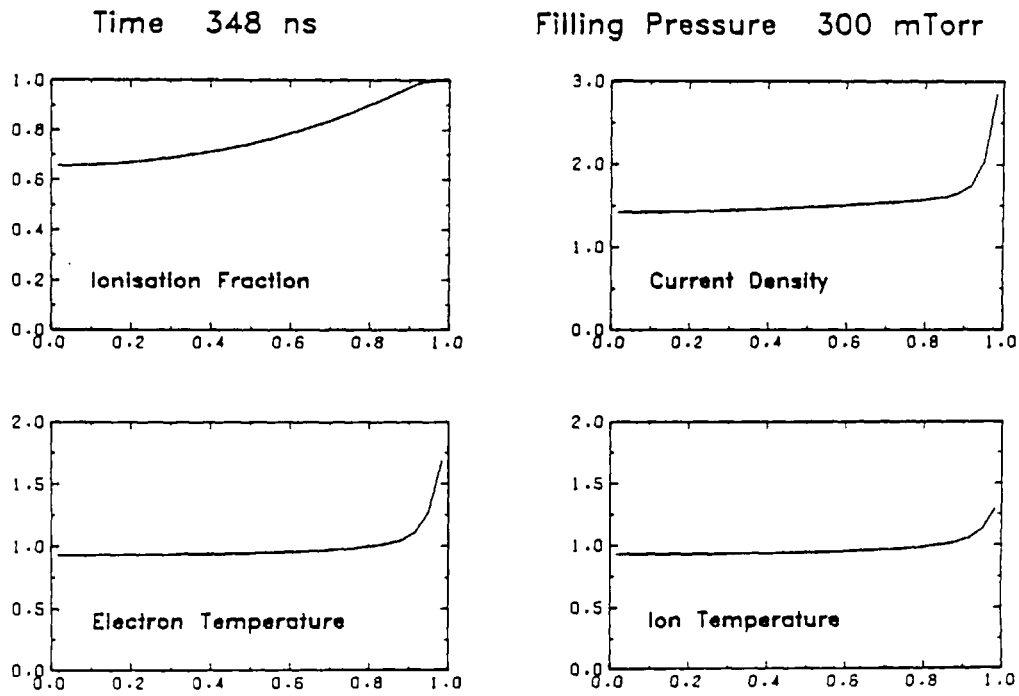


Fig 2.5 Ionisation fraction, current density, and temperature against radius

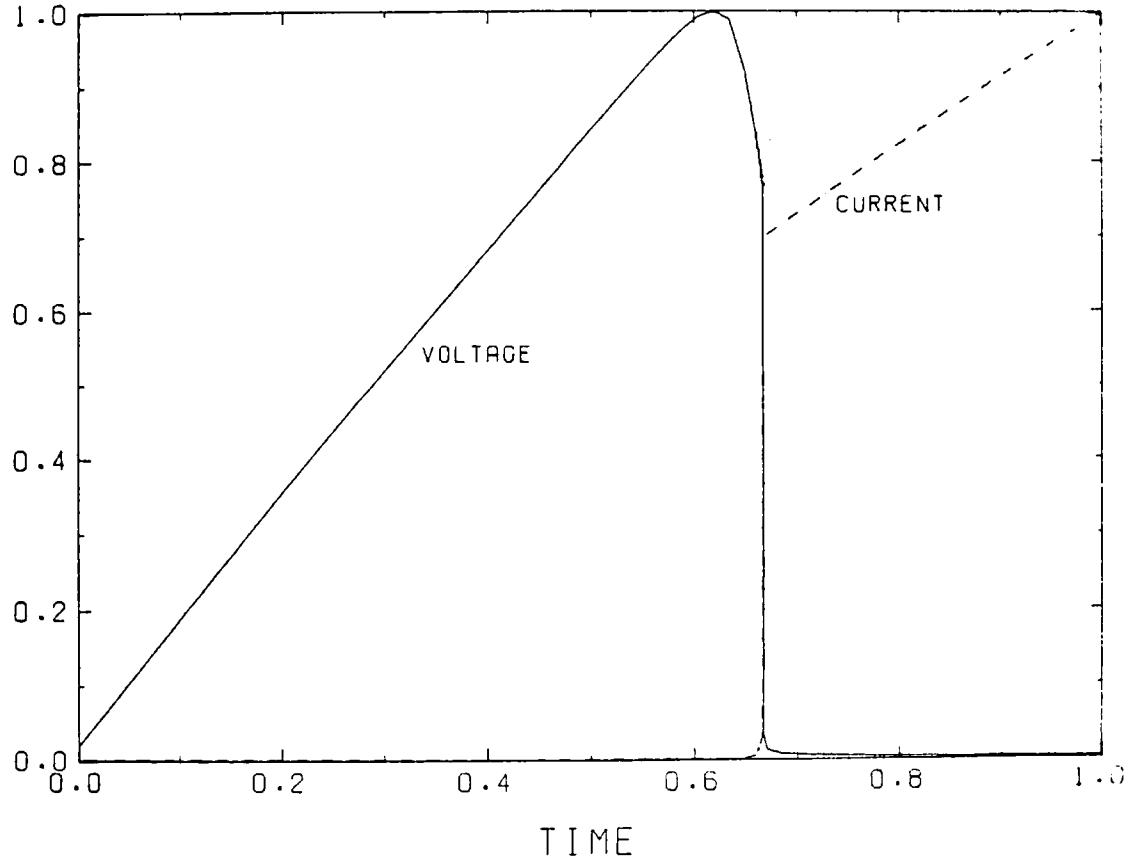


Fig 2.6 Current and voltage against time

Time = 215 ns

Filling Pressure = 80 mTorr

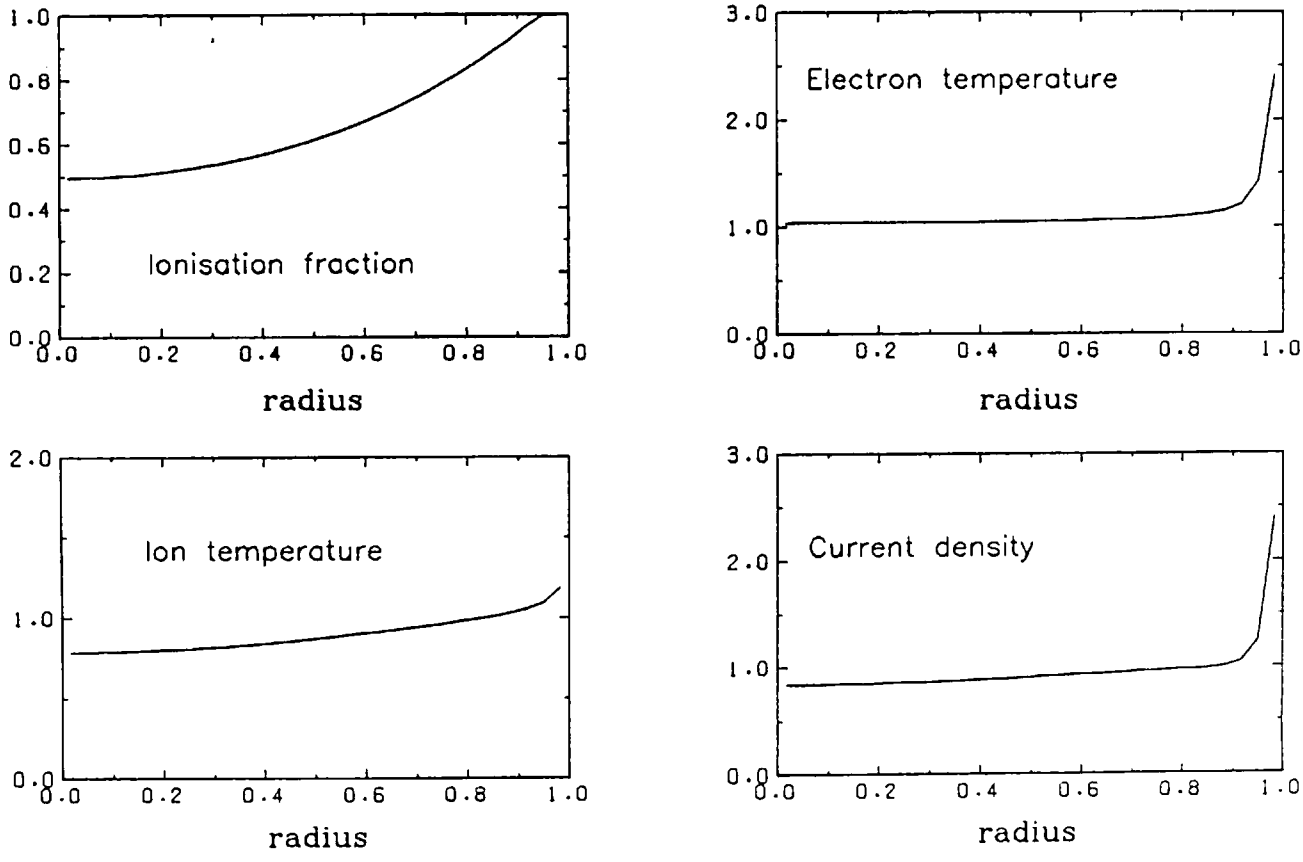


Fig 2.7 Ionisation fraction, current density, and temperature against radius

when the pinch is completely ionised at the edge. This "time to breakdown" agrees roughly with the experimentally observed time (Choi, 1981 private communication). The ionisation fraction varies from about 70% on axis to 100% at the boundary. The electron and ion temperatures are roughly equal at 1eV except in a boundary layer at the edge of the plasma.

In fig 2.7 the results are shown from a run in which the filling pressure was 80mTorr. In this case the plasma has ionised more quickly and the boundary layer at the edge is more pronounced. The ionisation fraction varies from about 50% on axis to 100% at the wall. At this filling pressure, the electron and ion temperatures are both still approximately 1eV.

In all the runs described in this chapter and in the runs used as initial conditions for the hydrodynamics programs, the initial ionisation fraction chosen was $f = 10^{-6}$. Killeen, Gibson and Colgate (1960) used $f = 10^{-2}$ in their program. Both these values are much higher than the equilibrium ionisation fraction calculated from the Saha equation. Changing the ionisation fraction initially would only be expected to change the time to breakdown and not the final result. For the 300 mTorr run changing the initial ionisation fraction to $f = 10^{-8}$ produced no significant change in the results and made virtually no difference to the time to breakdown.

As the filling pressure decreases to zero the breakdown time

calculated by the program also decreases to zero. This does not happen experimentally where the breakdown time starts to increase again below a certain filling pressure. This occurs as the assumptions implicit in the model (eg $n\lambda_D^3 >> 1$) start to break down.

2.6 Conclusions

In this chapter we have developed a program to model the preionising phase of a z-pinch. The equations used were those used by Killeen, Gibson and Colgate (1960) in a study of boundary layer formation, rewritten in cylindrical geometry. Using finite differences a parabolic partial differential equation governing magnetic field diffusion was solved. The current density coupled the diffusion equation to a set of ordinary differential equations at each mesh point, and these equations were solved using a Runge - Kutte scheme.

Results were obtained for a 1cm radius pinch at initial filling pressures of 80 and 300 mTorr. The electron and ion temperatures obtained were in agreement with rough experimental figures for the temperature. The results can be used in one of two ways :

(1) based on the program average values of electron and ion temperature and current density can be given as initial conditions to the programs described in chapter 4

or

(2) the profiles obtained from the program can be input as initial conditions to these programs.

CHAPTER 3

3.1 Introduction

One of the problems in modelling the formation of a z-pinch is the treatment of the "vacuum region" between the pinch and the wall. In this chapter we discuss the various methods for treating the vacuum region in MHD calculations. Hain's (1960) method is described first along with some additional work due to Lindemuth(1977). Other possible methods of treating the vacuum region are discussed briefly. A few of the experimental results on the behaviour of the low density "vacuum plasma" are discussed, and a physical picture in terms of magnetic flux and wall currents is obtained. This simple picture is developed and applied to a 1-D ideal Lagrangian simulation of the formation of a z-pinch. The results obtained show that the wall current model can have an appreciable effect on the pinch dynamics and that the model represents a possible explanation for the discrepancy between experimental results at Imperial College and the simulation described in Chapter 1. Finally the effect of varying γ is discussed, and it is shown that as γ decreases the amplitude of the bounce increases. Thus if a pinch is "dirty" and has a low value of γ a larger bounce after compression will be observed than if the pinch is clean.

3.2 Computational treatment of the vacuum region

Hain's method

Hain et al (1960) presented a comparison of a numerical simulation of pinch formation with experimental results. They used a one dimensional cylindrically symmetric two temperature MHD model and derived two schemes for solving the equations. In their paper they discuss in some detail the boundary conditions at the wall of the pinch vessel. The physical boundary condition is $v_r = 0$. However, if this boundary condition is imposed computationally, the plasma at the wall experiences the full electric field E and a current $j = \sigma E$ flows near the wall. This heats the plasma at the rate σE^2 and a singularity results with the temperature and electrical conductivity being extremely large and all the current flowing at the wall. This singularity would be removed by a full boundary layer treatment including enhanced transport coefficients (Roberts and Potter, 1970). However we can neglect the boundary layer effects by making the plasma move with the velocity of the lines of force $\underline{E} \times \underline{B}/B^2$, as a result of which the current will be zero since

$$\underline{E} + \underline{v} \times \underline{B} = 0$$

Hain et al (1960) chose to have plasma emitted continuously from the wall in their simulation. Thus their continuity equation became

$$\frac{\partial \rho}{\partial t} + \frac{1}{r}\frac{\partial}{\partial r}(r\rho v) = s(t)\,\delta\left(r-(r_{wall}-\epsilon)\right) \qquad (3.1)$$

where ϵ is small and positive . From this equation it can be seen that there is no conflict in the number of boundary conditions imposed since specifying ρ at the wall is equivalent to specifying s(t). Their requirements for the boundary conditions were that the plasma must emerge from the wall with the E/B drift velocity which should be determined by the main plasma , and that the rate of emission of background plasma must be such that inertial effects are small. They chose a value of 5% of the initial density for the background plasma density.

One problem they found in applying these boundary conditions was an instability associated with the kinetic pressure of the low density plasma. The total pressure on the pinch is given by

$$\left(\frac{B^2}{2} + \rho T + \tfrac{1}{2}\rho v^2\right)\Big|_{wall}$$

The instability arises because the $\frac{1}{2}\rho v^2$ term causes the pinch to move in faster, which increases v and hence $\frac{1}{2}\rho v^2$. The instability can be removed by rewriting the momentum equation so that

$$\frac{B^2}{2}(R) = \frac{B^2}{2}(R-\epsilon) + \tfrac{1}{2}\rho v^2$$

which ensures conservation of momentum.

Lindemuth (1977) has published a generalisation of Hain's method. Hain's method works well for fast pinches when the magnetic pressure $B^2/2\mu$ rapidly becomes much larger than the plasma pressure p.

Lindemuth reports that for slow pinches and reverse bias pinches, as well as for calculations where the current changes direction, the success of Hain's method is limited. He ascribes this to an incorrect treatment of the boundary condition at the wall. Lindemuth has generalised the ANIMAL (A New Implicit Magnetohydrodynamic ALgorithm) code so that when $p > B^2/2\mu$ there is no force on the plasma and separation from the wall does not occur. He does this by setting the force on the boundary

$$F_b = 0 \qquad \text{if } \tfrac{1}{2}(B_1+B_2)(B_2-B_1)+P_2 \geq 0 \text{ and } v_1 = 0$$

$$= \tfrac{1}{2}(B_1+B_2)(B_2-B_1)+P_2 \qquad \text{otherwise}$$

where 1 denotes a quantity at the boundary and 2 a quantity one mesh step in from the boundary. If and only if F_b is nonzero v_1 becomes nonzero and is set to

$$v_1 = \tfrac{3}{2}v_2 - \tfrac{1}{2}v_3 \tag{3.2}$$

When v_1 is inwards background plasma with a density ρ_{bg} and energy ϵ_{bg} is convected into the simulation region. Eq (3.2) ensures that the magnetic field is convected into the simulation region with the E/B drift. When v_1 is outwards, the background plasma and the magnetic field are convected out of the region until the density ρ_1 reaches some cutoff density which indicates that real plasma has reached the wall. v_1 is then reset to zero and F_b becomes zero again. When using this boundary condition, Lindemuth reports good agreement between results from the ANIMAL code and results from the Lagrangian code

HEMPMHD.

Other possible schemes for the vacuum region

In the FOCUS code, Roberts and Potter (1970) treated the vacuum region in a numerical simulation of the formation of a plasma focus by introducing a density ρ_{vac} such that when the density of the plasma fell below ρ_{vac} the conductivity was set to zero. It was then necessary to solve Laplace's equation for the magnetic field.

Another method for overcoming the problem of the high Alfven speed in the vacuum was proposed by Boris (1970) who introduced the displacement current into the MHD equations, and then introduced an artificially low speed of light. This approach does not seem to have been widely used.

Another possible method for treating the vacuum region is the Random Choice Method which has been used by Sod (1976) to investigate converging shocks in cylindrical symmetry. The Random Choice Method is a numerical method for solving nonlinear hyperbolic equations which is particularly useful when the solution contains shock waves and low energy densities. The solution is stepped forward in time by solving a set of Riemann problems with a random shift in space. The Random Choice Method is first order accurate in space but has infinite resolution and the method is based on a constructive existence proof by Glimm(1963).

One feature of particular interest in the Random Choice Method is its unconditional stability. If it is run at a Courant number higher than 1 the method changes the problem being solved so that the maximum speed on the mesh is just the mesh speed $\Delta x/\Delta t$. Thus the RCM has some similarities with the approach of Boris described above.

3.3 A simple Wall Current model of the vacuum plasma

Physical picture of vacuum plasma

In all the techniques for treating the vacuum region discussed above, the aim has been to reproduce the properties of a vacuum ($\sigma = 0$) by a computational artifice. Experimentally we know that low density plasma does exist in the "vacuum" region at a temperature of a few eV. At temperatures of a few eV the conductivity of the plasma is still high, and the behaviour of the plasma is not the same as the behaviour of a vacuum. Certainly, the current density will be small in both cases, but it will be small for different reasons. In a vacuum region $\sigma = 0$, and so $j = 0$ automatically. In a region of low density plasma $\underline{j} \times \underline{B} \simeq 0$ which implies that any currents will be force free. The difference between a vacuum and a low density plasma can be seen clearly by considering the behaviour of magnetic flux in each region. In a vacuum the flux changes almost instantaneously in response to changes in the external circuit; in a low density high conductivity plasma, the flux is "frozen - in" to the plasma and changes in the external circuit move the plasma. Thus if we consider the collapse of

a pinch occurring on a timescale which is fast compared with the resistive diffusion time through the low density plasma, we see that after collapse magnetic flux will be trapped between the magnetic piston and the wall. This effect, which has not been included in any previous model of pinch formation, can have an important effect on the pinch dynamics.

Experimental evidence for vacuum plasma

Kvartskhava et al (1971) have published results on z-pinch experiments which clearly demonstrate discharges on the walls of the z-pinch vessel at the time of maximum compression. They obtained measurements of current density as a function of radius at different times during the discharge. In particular, when the pinch is collapsing they find that there is a reverse current outside the pinch boundary and a forward current at the wall. In a later paper (1974) Kvartskhava et al present further experimental evidence of breakdown near the wall and propose a method of freezing the working gas at the wall of the discharge vessel to avoid impurities entering the plasma when breakdown occurs near the wall. They also present results from a numerical model in which they consider the effect of the breakdown at the wall. They use a one dimensional model of a z-pinch and allow for the breakdown plasma by adding a multiple λM_o of the original pinch mass M_o at the wall. They give very few details of their calculations and simply state that for $\lambda \simeq 1$ virtually no effect is observed, whereas for $\lambda \simeq 10$ the results agree very well with

experiment, and present a curve of piston position against time which looks similar to the ones to be presented later on. In the model presented here, this dependence on the mass at the wall is not found, and on physical grounds it is difficult to see why there should be much dependence on the mass.

A simple model for behaviour of vacuum plasma

We have seen that the experimental picture of the formation of a pinch is that there is no "vacuum" as such, but rather a low density region and a high density region which both have a high conductivity, Furthermore, as the pinch nears maximum compression the radiation from the pinch is sufficient to vaporise some of the discharge vessel wall. Thus as the pinch collapses the plasma in the low density region will drift towards the axis with the E/B drift. Since the resistivity is independent of density, and the low density plasma is at a temperature of a few eV, the low density region will be a highly conducting plasma in which the current density is zero because inertia is negligible. On timescales short compared with the resistive diffusion time the magnetic flux will be "frozen-in" to the plasma, and the field lines will move with the plasma. Thus, avoiding the problem caused by a high Alfven speed in the "vacuum" region by introducing plasma at the wall so that the density never falls below some minimum value is quite reasonable on physical grounds. However, care must be taken to ensure that the plasma introduced in the "vacuum" region behaves in the same

way that the real low density plasma does. When the pinch is collapsing this is effected by allowing plasma to drift in through the wall at the E/B drift, and this is what is done in most computer simulations. If the plasma is allowed to drift out through the wall the conservation of flux is not satisfied and the simulation is not modelling the real plasma correctly.

The physical picture we have when constructing the wall current model is that when the pinch is collapsing there will be plasma left behind in the low density region - either left behind by the magnetic piston or as a result of outgassing from the wall or perhaps burnt off the wall by the intense radiation from the pinch near maximum compression. Thus we imagine plasma created at the wall and drifting in with the magnetic flux frozen in to it. When the pinch starts to expand the "vacuum" plasma will drift out to the wall taking the magnetic flux with it. It will not be able to drift through the wall however and thus the magnetic flux cannot escape.

We can express this mathematically quite simply. If we write the magnetic flux as

$$\Phi = \int_{r_p}^{r_w} B \, dr \qquad (3.3)$$

and use Ohm's law

$$E = -vB \qquad (3.4)$$

we can see that

$$\frac{d\Phi}{dt} = -B(r_p)\frac{dr_p}{dt} + \int_{r_p}^{r_\omega} \frac{\partial B}{\partial t}\, dr \qquad (3.5)$$

$$\therefore \quad \frac{d\Phi}{dt} = -v(r_\omega)B(r_\omega) \qquad (3.6)$$

and so $d\Phi/dt \geq 0$ is equivalent to $v \leq 0$ at $r = r_{wall}$

To summarise, we have shown that the conventional treatment of the vacuum region does not model the physical behaviour of the plasma all the time and we have derived a model using simple physical concepts which will lead to a better treatment of the vacuum region. We have also shown that the model can be expressed in either of two equivalent forms, ie

$$\frac{d\Phi}{dt} \geq 0 \qquad (3.7)$$

or

$$v_{wall} \leq 0 \qquad (3.8)$$

3.4 A simple computer program including the wall current model

In order to see what effect the wall current model has, a simple program was written to model the formation of a z-pinch in cylindrical

symmetry including the effect of wall currents. A simple ideal MHD model with a sheet current was chosen, and the equations solved were

$$\frac{\partial \rho}{\partial t} + \frac{1}{r}\frac{\partial}{\partial r}(r\rho v) = 0 \tag{3.9}$$

$$\frac{\partial \rho}{\partial t} + \frac{1}{r}\frac{\partial}{\partial r}(r\rho v^2) = -\partial p/\partial r \tag{3.10}$$

$$\frac{d}{dt}\left(p/\rho^{\gamma}\right) = 0 \tag{3.11}$$

The magnetic field was given by

$$B = 0 \qquad r \leq r_p(t) \tag{3.12}$$

$$= I/r \qquad r > r_p(t)$$

and the boundary conditions were

$$v = 0 \qquad \text{at } r = 0 \tag{3.13}$$

$$p = B^2/2 \qquad \text{at } r = r_b(t) \tag{3.14}$$

The equation of motion of the pinch boundary was

$$\frac{dr_p}{dt} = v_p \tag{3.15}$$

with v_p determined by extrapolation.

These equations were solved on a Lagrangian mesh using the FCT technique of Boris and Book (1973). The FCT routines allow the grid to move with a grid velocity u^g_i which is specified by the user. The grid is moved using

$$r_i^{n+1} = r_i^n + u^g_i \Delta t \tag{3.16}$$

The simplest and most obvious choice of u^g_i is

$$u^g_i = v_i^{n+1/2} \tag{3.17}$$

This choice was the first used in the simple model described in this chapter. For stability the usual CFL condition must be satisfied

$$\Delta t \leq .5 \min\{\Delta r_i / v_i\} \tag{3.18}$$

When the program was run it was found that despite the first order diffusion near steep gradients which removes the necessity for a von Neumann type artificial viscosity term (Craxton and McCrory (1979)), the points at the shock front became extremely close causing the timestep to become vanishingly small. Examination of the way quantities are differenced in FCT showed that the problem was caused because the FCT routines do not "see" the small mesh size. Fig 3.1 shows the finite difference mesh around the shock front. The pressure

gradient at point i is given by

$$\nabla p_i = (p_{i+1/2} - p_{i-1/2})/(r_{i+1/2} - r_{i-1/2}) \qquad (3.19)$$

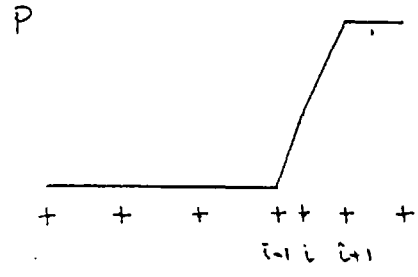


Fig 3.1 Finite difference mesh near shock front

where $p_{i+1/2} = \frac{1}{2}(p_i + p_{i+1})$

$r_{i+1/2} = \frac{1}{2}(r_i + r_{i+1})$

and therefore $\nabla p_i = (p_{i+1} - p_{i-1})/(r_{i+1} - r_{i-1})$

Thus there is no direct coupling between ∇p_i or any other physical quantity and the distance $r_{i+1} - r_i$. Having identified the problem, it was solved by moving the points $r_{i+1/2}$ with the fluid velocity $v_{i+1/2}$ Thus we set

$$r_{i+1/2}^{n+1} = r_{i+1/2}^{n} + \Delta t\, v_{i+1/2}^{n+1/2}$$

and

$$r_i^{n+1} = \frac{1}{2}\left(r_{i+1/2}^{n+1} + r_{i-1/2}^{n+1}\right)$$

$$= \Delta t\, v_i^{n+1/2} + \frac{1}{4}\left(r_{i+1}^{n} + 2r_i^{n} + r_{i-1}^{n}\right)$$

This can be written as

$$r_i^{n+1} = r_i^{n} + \Delta t\, v_i^{n+1/2} + \frac{1}{4}\left(r_{i+1}^{n} - 2r_i^{n} + r_{i-1}^{n}\right) \qquad (3.20)$$

and it can be seen that we are adding a diffusive term $\frac{1}{4\Delta t}\frac{\partial^2 r}{\partial i^2}$.

Craxton and McCrory (1979) have published a similar technique for rezoning in FCT. Their idea is to make the rezoning as nearly Lagrangian as possible by calculating the masses M_i in each cell and requiring the grid to move in such a way that the mass in each cell M_i remains constant. They define interface positions $y_{i+1/2}$ with the grid initially given by

$$r_i^{0} = \frac{1}{2}\left(y_{i+1/2} + y_{i-1/2}\right)$$

The products $M_i = \rho_i^{0}\,\Delta V_i^{0}$ are calculated and stored, and as the grid moves the new interface positions are calculated from

$$\Delta V_i^{n+1} = M_i/\rho_i^{n+1}$$

using the appropriate expression for ΔV_i in terms of y_i, y_{i+1}. The new grid points are then calculated from

$$r_i^{n+1} = \frac{1}{2}\left(y_{i+1/2}^{n+1} + y_{i-1/2}^{n+1}\right)$$

Since this is an ideal model, eqs (3.9) - (3.11) keep their form when we change to non - dimensional variables. In order to implement the wall current model it only remains to specify the current I.

The magnetic flux

$$\underline{\Phi} = \int_{r_p}^{1} B\,dr \qquad (3.21)$$

$$= -I \log r_p$$

where B = I / r in non - dimensional variables, and $r_{wall} = 1$.

If we write the current through the pinch as $I = I_o + I_w$, where I_o is the current in the external circuit and I_w is the wall current, the the flux $\underline{\Phi}$ is given by

$$\underline{\Phi} = -(I_o + I_w) \log r_p \qquad (3.22)$$

Assuming for the moment that I_o is constant we find

$$\frac{d\underline{\Phi}}{dt} = -\frac{(I_o + I_w)}{r_p}\frac{dr_p}{dt} - \log r_p \frac{dI_w}{dt} \qquad (3.23)$$

When the pinch is collapsing $dr_p/dt < 0$ and $d\underline{\Phi}/dt > 0$ with $I_w = 0$. When the pinch starts to expand the term $-(I/r_p)\,dr_p/dt$ becomes negative and $d\underline{\Phi}/dt = 0$ giving

$$\frac{dI_w}{dt} = -\frac{(I_o + I_w)}{r_p \log r_p}\frac{dr_p}{dt} \qquad (3.24)$$

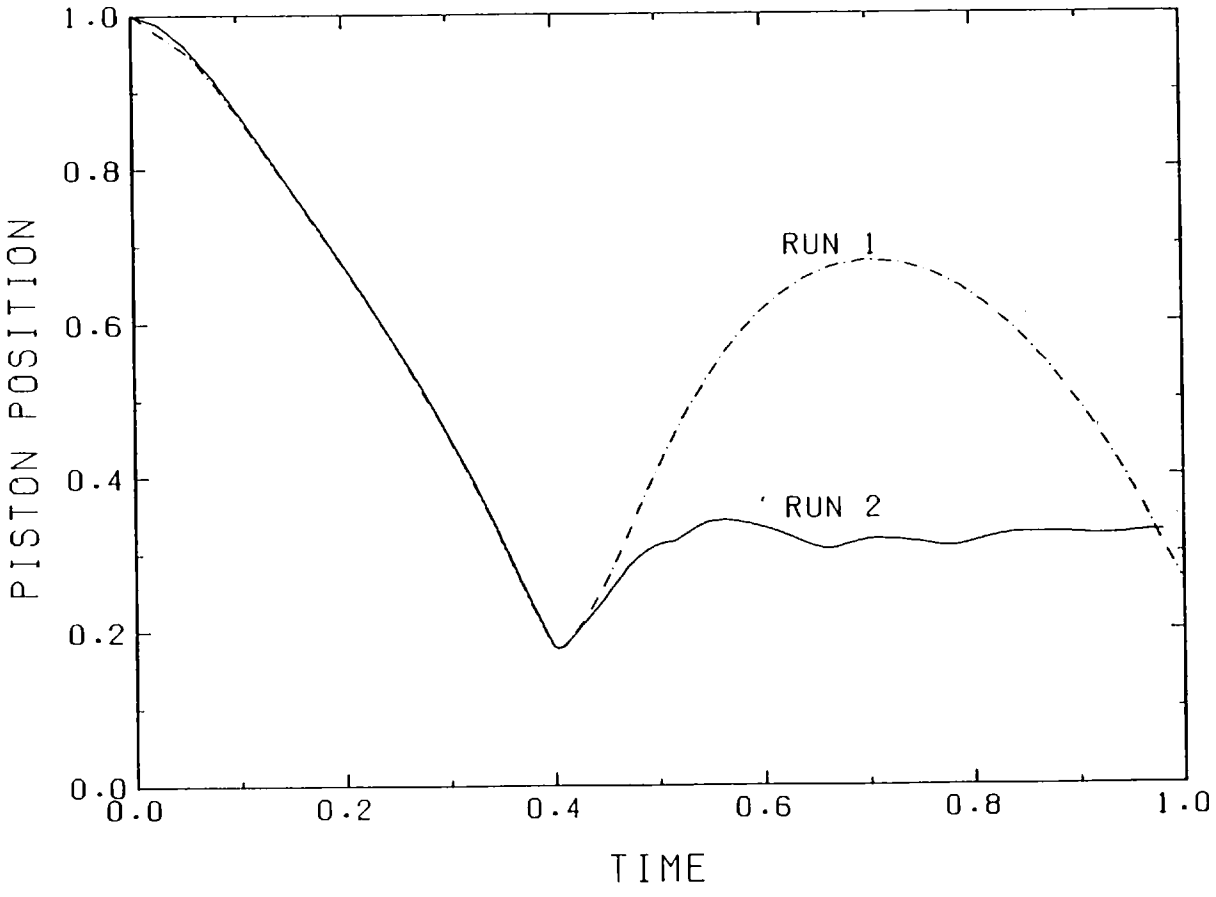


Fig 3.2 Piston position vs time with and without wall currents for $I_o = 3$

It can be seen from this equation that this is a self limiting process.

3.5 Results from the simple model

To illustrate the results from this model, the program was used to simulate the formation of a fast z-pinch driven by a constant current. A logical switch was included in the program described in the previous section so that the wall current could be turned on and off. The results shown in fig 3.2 are from a run in which a constant non-dimensional current $I_o = 3$ was used. Run 1 shows the piston position as a function of time when the wall current was switched off. After compression the piston bounces out to about .7 of the wall radius. In run 2, the wall current has been switched on and the large bounce after compression has been prevented, with the piston coming to rest at a radius of about .3 times the wall radius. The magnitude of the wall current can be calculated from eq(3.22) and is found to be about .15 of the main pinch current. From the results presented here we can see that the wall current model can remove the bounce after compression observed in previous numerical simulations of pinch formation (Christie, 1981).

3.6 Effect of varying γ

The results presented above were for $\gamma = 5/3$. The effect of varying γ can be calculated fairly easily using the ideas developed in the previous sections. The total energy in the pinch vessel is given by

$$E = \int_0^1 \left(\frac{p}{\gamma - 1} + \frac{B^2}{2} + \frac{1}{2} \rho v^2 \right) 2\pi r \, dr = \frac{\overline{p}}{\gamma - 1} \pi r_p^2 + \frac{1}{2} \underline{\Phi} I + \overline{T} \qquad (3.25)$$

where T is the kinetic energy, $\underline{\Phi}$ is the magnetic flux, I is the current and r_p the pinch radius. Neglecting radiation loss and joule heating $\partial E / \partial t = 0$ and so

$$\frac{\overline{p}}{\gamma - 1} \pi r_p^2 + \frac{1}{2} \underline{\Phi} I + \overline{T} = \text{const}$$

With the wall current model $\underline{\Phi}$ = const, $I = -\underline{\Phi} / \log r$ and so taking $p \propto \rho^\gamma$ with $\rho \propto 1/r$

$$E = \frac{A}{r^{2(\gamma-1)}} - B / \log r$$

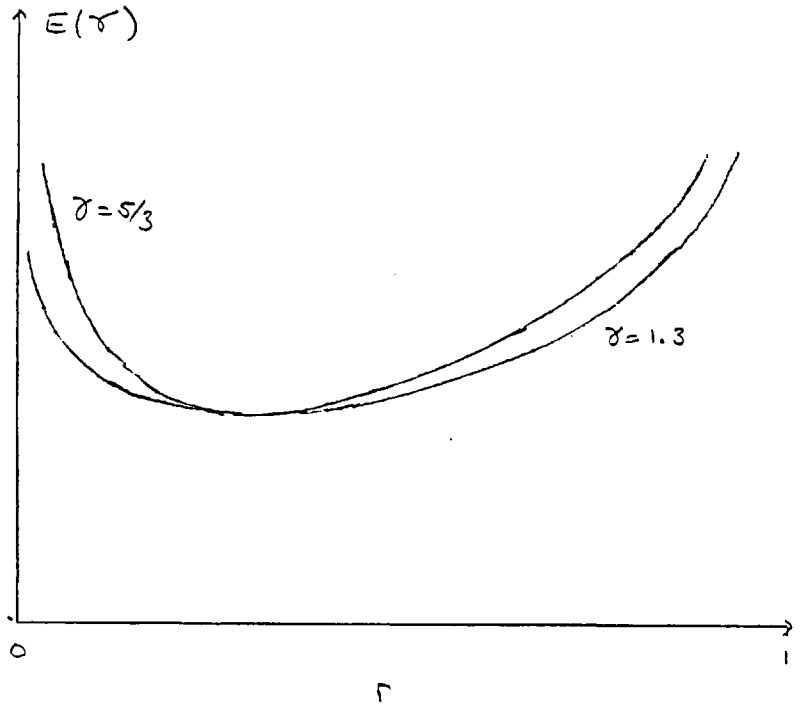


Fig 3.3 $E(\gamma)$ vs γ for two values of γ

For a given E this has two values r_1, r_2 of r where T = 0 and the difference between these solutions $|r_1 - r_2|$ gives the amplitude of the bounce. In fig (3.3) the expression

$$\frac{A}{r^{2(\gamma-1)}} - \frac{B}{\log r}$$

is plotted for various values of γ.

The effect of varying γ is of interest because it could account for cases where a bounce is observed after compression in a z-pinch. If we consider a pinch with impurities then the number of degrees of freedom of the plasma is increased and the effective γ =n+2/n decreases. From the graphs we can see that decreasing does "stretch out" the graphs a bit. However it should be realised that it is difficult to compare like with like here because decreasing γ would mean that the pinch would collapse further for the same initial conditions. We have the choice of comparing results for the same initial conditions or of comparing results for the same minimum radius. It can be seen though, that in either case decreasing γ will increase the size of the outward bounce.*

3.7 Conclusion

In this chapter we have explored the computational modelling of the vacuum region. We examined the physical and computational boundary conditions used in Hain's 1960 model of pinch formation. The effect of the vacuum plasma introduced at the wall was discussed and related to the physical effects near the wall. From experimental evidence we

* However, impurities will also increase the resistivity of the low density plasma and allow flux to diffuse out more quickly, thus increasing the size of the bounce. This effect is ignored.

know that a low density plasma exists in the vacuum region. Because inertial effects are small the field in the vacuum region is force free; as the pinch collapses, magnetic flux and low density plasma are driven in together from the wall. Because the resistivity does not depend on the density, the resistive diffusion time through the "vacuum plasma" is longer than the other timescales of interest and the magnetic flux is "frozen-in" to the plasma.

Taking the idea that the flux is frozen in to the plasma, we showed that by taking the physically reasonable boundary condition of only allowing plasma to be driven in from the wall, the magnetic flux cannot decrease. In contrast to previous numerical models this introduces an asymmetry and so an expanding pinch does not behave in the same way as a collapsing pinch.

By including the effect of this wall current model in a very simple ideal simulation we found that the effect of the low density plasma can have a significant effect on the dynamics of pinch formation. The wall current model reduces the large bounce after compression and leads to qualitative agreement with experiments.

Finally we considered the effect of varying γ and showed that a low value of γ will produce a larger bounce than a higher value. This represents a possible explanation for some of the early experiments where a large bounce was observed.

CHAPTER 4

4.1 Introduction

In this chapter we include the wall current model described in the previous chapter in a more realistic MHD program. Qualitative agreement with experiment has been obtained by means of the simple model described in the previous chapter; in this chapter we aim to achieve quantitative agreement with experiment.

In section 4.2 we discuss the MHD equations for pinch formation in dimensionless form. We consider the two temperature MHD equations with the effects of resistivity, viscosity, electron and ion thermal conductivity and equipartition included. The bremsstrahlung radiation loss term is included in the electron energy equation along with Joule heating. Viscous heating is included in the energy equation for the ions.

In section 4.3 the method of solution of the equations using Flux Corrected Transport is described. The solution procedure is split into two stages:

(1) solve for the effect of convection explicitly using FCT

(2) solve for the effect of all the nonideal terms fully implicitly.

In stage (1) the transport algorithm can be either Eulerian or Sliding

Rezone. In the first case the vacuum plasma is modelled explicitly and the wall current model is implemented by only allowing inward flow at the outer boundary. Using this method the resistive diffusion of flux through the boundary is modelled properly, but the pinch structure on axis is not resolved efficiently. In the sliding rezone calculations the pinch structure is well resolved, but the resistive diffusion of flux through the vacuum plasma and wall is not treated. This restriction was subsequently removed, and agreement between the methods is obtained.

Section 4.4 describes a more detailed wall current model than that given in chapter 3. The effect of diffusion of flux through the layer of plasma at the wall is included. This leads to an extra term in the equation representing the loss of flux through the wall.

Section 4.5 presents the results from the MHD program described in the previous sections. Graphs of the plasma properties and of the piston position as a function of time are shown. At 80 mTorr the results agree with experiment and the previous simulation described by Hopkins et al (see section 1.5). At 300 mTorr, where Hopkins et al were unable to match experiment, we obtain good agreement with the experimental results.

Recent work by Maxon and Nielsen (1981a, 1981b) has proceeded along similar lines to the work described here. They have modelled the formation of a capacitor bank driven z-pinch at Livermore using both

Lagrangian and Eulerian codes in one dimension. They use an empirical equation of state for hydrogen, and find that the distance between shock and piston decreases in their work, with the density jump increasing. They obtain the best results from the Lagrangian simulation.

4.2 MHD equations for pinch formation

In this section the MHD equations used in modelling the formation of a z-pinch are discussed. The assumptions made are that the plasma is fully ionised and that all quantities depend only on the radius r and time t. A two temperature model is used with Ohmic heating and bremsstrahlung loss applying to the electrons and viscous heating to the ions. In addition the electron and ion temperatures are coupled through the equipartition term.

The assumptions stated above can be justified as follows:
From the nature of the z-pinch the formation is inherently one dimensional provided the "aspect ratio" (length/radius) is fairly large.
From the results of the STARTUP program described in chapter 2, it can be seen that the plasma is fully ionised at the edge of the pinch and about 70% ionised at the centre. The maximum temperature change to be expected as a result of including compressional ionisation would be of the order of

ionisation energy * (%unionised) $\simeq$ 1eV

This is so small that it is not worth including an ionisation calculation in the program.

If we consider a two fluid model in one dimension and assume quasineutrality ($n_e = n_i = n$, for $Z = 1$) then using the continuity equation for electrons and ions we find that

$$\nabla \cdot n(\underline{v}_e - \underline{v}_i) = 0$$

Since $v_e = v_i$ on axis, the velocities are equal everywhere and we need only consider a two temperature model.

We consider the formation of a z-pinch in which the motion is predominantly radial. Only the θ component B_θ of the magnetic field is allowed. The MHD equations can be written in non dimensional form as

$$\frac{\partial \rho}{\partial t} + \nabla \cdot (\rho \underline{v}) = 0 \tag{4.1}$$

$$\frac{\partial \rho \underline{v}}{\partial t} + \nabla (\rho \underline{v}\underline{v}) = -\nabla p + \underline{j} \times \underline{B} + \nabla \cdot \underline{\underline{\tau}} \tag{4.2}$$

$$\frac{\partial p_e}{\partial t} + \nabla \cdot p_e \underline{v} = (\gamma - 1)\left\{ - p_e \nabla \cdot \underline{v} + \eta j^2 + \nabla \cdot (\hat{\kappa}_e \nabla \theta_e) - \hat{P}_{rad} \right\} + \frac{p_i - p_e}{\hat{\tau}_{eq}} \tag{4.3}$$

$$\frac{\partial p_i}{\partial t} + \nabla \cdot p_i \underline{v} = (\gamma - 1)\left\{ - p_i \nabla \cdot \underline{v} + \hat{\mu} (\nabla \cdot \underline{v})^2 + \nabla \cdot (\hat{\kappa}_i \nabla \theta_i) \right\} + \frac{p_e - p_i}{\hat{\tau}_{eq}} \tag{4.4}$$

$$\frac{\partial \underline{B}}{\partial t} = \nabla \times (\underline{v} \times \underline{B}) - \nabla \times \left(\hat{\eta} \nabla \times \underline{B}\right) \tag{4.5}$$

where the dimensional quantities are obtained from the non dimensional quantities by

$$\rho_D = \rho_0 \rho \qquad p_D = p_0 p$$

$$\underline{v}_D = v_0 \underline{v} \qquad \underline{j}_D = j_0 \underline{j}$$

$$r_D = r_0 r \qquad \underline{B}_D = B_0 \underline{B}$$

$$t_D = t_0 t$$

and the following relations hold between the dimensional constants

$$v_0 = r_0 / t_0 \tag{4.6}$$

$$p_0 = \rho_0 v_0^2 \tag{4.7}$$

$$B_0^2 = \mu_0 p_0 \tag{4.8}$$

$$j_0 = B_0 / \mu_0 r_0 \tag{4.9}$$

where $\mu_0 = 4\pi . 10^{-7} H m^{-1}$, and

$$\hat{\eta} = \frac{\eta}{\mu_0 r_0 v_0} \tag{4.10}$$

is the inverse of the magnetic Reynolds number, and

$$\hat{\mu} = \frac{\mu}{\rho_0 r_0 v_0} \tag{4.11}$$

is the inverse of the Reynolds number. The non-dimensional equipartition time is $\hat{\tau}_{eq} = \tau_{eq}/t_0$, and the non-dimensional bremsstrahlung radiation loss is

$$\hat{P}_{rad} = \frac{t_0}{p_0} P_{rad} \tag{4.12}$$

We now consider only one-dimensional motion, with all quantities depending only on the radius. We let v be the radial velocity, and B be the θ component of the magnetic field. Eqs(4.1) to (4.5) become

$$\frac{\partial \rho}{\partial t} + \frac{1}{r}\frac{\partial}{\partial r}(r\rho v) = 0 \tag{4.13}$$

$$\frac{\partial \rho v}{\partial t} + \frac{1}{r}\frac{\partial}{\partial r}(r\rho v^2) = -\frac{\partial p}{\partial r} + jB + \frac{\partial}{\partial r}\left(\mu \frac{\partial v}{\partial r}\right) \tag{4.14}$$

$$\frac{\partial p_e}{\partial t} + \frac{1}{r}\frac{\partial}{\partial r}(r p_e v) = -(\gamma-1)\left\{ p_e \nabla\cdot\underline{v} + \hat{\eta} j^2 + \frac{1}{r}\frac{\partial}{\partial r}\left(r \hat{\kappa}_e \frac{\partial \theta_e}{\partial r}\right) - P_{rad} \right\} + (p_i - p_e)/\hat{\tau}_{eq} \tag{4.15}$$

$$\frac{\partial p_i}{\partial t} + \frac{1}{r}\frac{\partial}{\partial r}(r p_i v) = -(\gamma-1)\left\{ p_i \nabla\cdot\underline{v} + \hat{\mu}(\nabla\cdot\underline{v})^2 + \frac{1}{r}\frac{\partial}{\partial r}\left(r \hat{\kappa}_i \frac{\partial \theta_i}{\partial r}\right) \right\} + (p_e - p_i)/\hat{\tau}_{eq} \tag{4.16}$$

If the drift parameter $j/(n_e c_s) \gtrsim 1$ and $T_e >> T_i$, then ion-sound turbulence will occur, and anomalous transport coefficients must be used. In the runs described here, the maximum value of the drift parameter was 0.18, and therefore ion-sound turbulence is not expected to be a major problem.

$$\frac{\partial B}{\partial t} + \frac{1}{r}\frac{\partial}{\partial r}(rvB) = -\frac{vB}{r} + \frac{\partial}{\partial r}\left(\frac{\hat{\eta}}{r}\frac{\partial}{\partial r}rB\right) \tag{4.17}$$

In this form, eqs (4.13) to (4.17) can be solved by Flux Corrected Transport.

Transport coefficients

Classical values* of the transport coefficients are used. Expressions for the transport coefficients in a hydrogen plasma are given by Potter (1973).

$$\eta = \frac{m_e \nu_{ei}}{ne^2} \tag{4.18}$$

$$\mu = \frac{nkT_i}{\nu_{ii}} \tag{4.19}$$

$$\kappa_e = \frac{5nk^2T_e}{m_e \nu_{ei}} \tag{4.20}$$

$$\kappa_i = \frac{5nk^2T_i}{m_i \nu_{ii}} \tag{4.21}$$

$$\tau_{eq} = \frac{m_i}{2m_e \nu_{ei}} \tag{4.22}$$

where n is the number density (electron and ion number densities are equal from quasi-neutrality), ν_{ei} , ν_{ii} are the electron-ion and ion-ion

* see opposite

collision frequencies and T_e, T_i are the electron and ion temperatures in MKS units. k is Boltzmann's constant and m_e, m_i are the electron and ion massses, and ν_{ei}, ν_{ii} are given by eqs (2.8), (2.9)

$$\nu_{ei} = \frac{n_e Z e^4 \log\Lambda}{25.8\pi^{1/2}\epsilon_0 m_e^{1/2} T_e^{3/2}} \tag{4.23}$$

$$\nu_{ii} = \frac{n_i Z e^4 \log\Lambda}{25.8\pi^{1/2}\epsilon_0 m_i^{1/2} T_i^{3/2}} \tag{4.24}$$

If we express the temperatures θ_e, θ_i in eV, eqs (4.18) - (4.22) become

$$\eta = 1.084 \cdot 10^{-4} \log\Lambda / \theta_e^{3/2} \tag{4.25}$$

$$\mu = 2.365 \cdot 10^{-6} \theta_i^{5/2} / \log\Lambda \tag{4.26}$$

$$K_e = 4.177\, \theta_e^{5/2} / \log\Lambda \tag{4.27}$$

$$K_i = 9.758 \cdot 10^{-2} \theta_i^{5/2} / \log\Lambda \tag{4.28}$$

The parameters w_e, w_i vary as functions of both radius and time during the simulation. The maximum values of w_e, w_i when considered as functions of radius are typically (at peak compression)

$$\max_{r_i} \{ w_e \} = 51.07$$

$$\max_{r_i} \{ w_i \} = 2.48$$

The E/B drift is typically $1.53\,10^5 ms^{-1}$

$$\tau_{eq} = \frac{5.899 \cdot 10^{-13}\, \theta_e^{3/2}}{\rho \log \Lambda} \tag{4.29}$$

The transport coefficients perpendicular to a magnetic field are smaller by a factor $1/(1+(\omega\tau)^2)$, where ω is the appropriate gyrofrequency and τ the appropriate collision time. Therefore the values of thermal conductivity and viscosity are given by

$$K_e^{\perp} = K_e^{''}/(1+w_e^2) \tag{4.30}$$

$$K_i^{\perp} = K_i^{\wedge}/(1+w_i^2) \tag{4.31}$$

$$\mu^{\perp} = \mu^{''}(1+w_i^2)/(1+4w_i^2) \tag{4.32}$$

with w_e, w_i given by

$$w_e = \frac{eB}{m_e \nu_{ei}} \tag{4.33}$$

$$w_i = \frac{eB}{m_i \nu_{ii}} \tag{4.34}$$

Using eqs (4.23), (4.24) these become

$$w_e = 4.469 \cdot 10^{-6}\, B\, \theta_e^{3/2}/\rho \tag{4.35}$$

$$w_i = 1.144\ 10^{-7}\ \beta\ \theta_i^{3/2}/\rho \tag{4.36}$$

4.3 Method of solution

We solve eqs (4.13) to (4.17) numerically using the FCT technique of Boris and Book (1973). Either a fixed or a sliding rezone mesh is used. When the sliding rezone mesh is used, the outer boundary is moved with the plasma velocity, and equal mesh spacing is taken inside the plasma. Changing from one version of the program to the other is straightforward because of the modular construction of the program. All variables are defined at N points in the interval (0,1) defined by

$$r_i = (i-1/2)\,\Delta r \tag{4.37}$$

with

$$\Delta r = 1/N \tag{4.38}$$

The variables describing the plasma at each point r are the density ρ, pressure p, electron temperature θ_e, ion temperature θ_i, magnetic field β, and current j. To define all the dimensional constants we can choose three of the seven numbers $r_0, t_0, v_0, \rho_0, p_0, B_0, j_0$. The characteristic parameters chosen are the initial radius r_0 (so that the non-dimensional radius is 1), the initial density ρ_0 (so that ρ = 1 initially) and we choose

$$p_0 = \frac{\rho_0 k}{2 m_H}$$

so that the non-dimensional temperatures correspond to the temperature in eV. The rest of the dimensional constants are then defined by eqs(4.6) - (4.9)

The next step is to initialise the plasma variables. Two options are allowed here. In the first option realistic values are chosen for the temperature and for the preionising current, and both are assumed uniform across the pinch. The magnetic field then rises linearly with r. In the second option the STARTUP program described in chapter 2 is run and the final profiles of temperature and magnetic field are stored on a binary file. The profiles are then read in from the binary file as initial data for the program which follows the collapse of the pinch.

Having initialised the variables, and set up the grid the program starts the loop over timesteps. Since FCT is an explicit scheme, a CFL condition must be satisfied on the timestep. Boris (1976) gives the condition on the timestep as

$$u\Delta t/\Delta x < 0.5 \qquad (4.39)$$

We run at a Courant number of .1 The sequence of calls to FCT subroutines is essentially the same as table 3 in (Boris, 1973)

Resistivity and viscosity

The effects of resistivity and viscosity are calculated by a fully

It should be noted that the expression used here for the viscous stress tensor is approximate. The sheared motion arising from the coupling of the r and z components of the stress tensor has been ignored, and in addition the assumption of weak curvature has been made. Thus we have approximated

$$(\nabla\cdot\underline{\underline{\tau}})_r = -\frac{1}{r}\frac{\partial}{\partial r}\left(r\left[\frac{1}{3}\mu r^2\frac{\partial}{\partial r}\left(\frac{v}{r^2}\right) + \frac{\mu}{1+4\omega_i^2}\frac{\partial v}{\partial r}\right]\right) - \frac{2}{3}\mu\frac{\partial}{\partial r}\left(\frac{v}{r^2}\right)$$

by

$$(\nabla\cdot\underline{\underline{\tau}})_r \simeq -\frac{\partial}{\partial r}\left[\frac{4}{3}\mu\,\frac{1+\omega_i^2}{1+4\omega_i^2}\frac{\partial v}{\partial r}\right]$$

implicit scheme to avoid inaccuracies when the timestep becomes large compared with the diffusion time (Craxton, 1976). Consider the equation for viscous diffusion

$$\frac{\partial v}{\partial t} = \frac{1}{\rho}\frac{\partial}{\partial r}\left(\mu \frac{\partial}{\partial r} v\right) \tag{4.40}$$

If we difference this equation fully implicitly, allowing for spatial dependence of the coefficients, we obtain

$$-\alpha_i v_{i+1}^{n+1} + \beta_i v_i^{n+1} - \gamma_i v_i^{n+1} = v_i^n \tag{4.41}$$

where

$$\alpha_i = \frac{\Delta t}{\Delta r^2}\left(\frac{\mu_{i+1}+\mu_i}{\rho_i}\right) \tag{4.42}$$

$$\gamma_i = \frac{\Delta t}{\Delta r^2}\left(\frac{\mu_i+\mu_{i-1}}{\rho_i}\right) \tag{4.43}$$

and

$$\beta_i = 1 + \alpha_i + \gamma_i \tag{4.44}$$

The boundary condition of $v = 0$ at $r = 0$ is obtained by setting $v_0 = -v_1$, and the boundary condition at $r=r_{wall}$ is chosen to be $\gamma_n = 0$. This leaves the value of v_n unchanged from the E/B drift. Resistive diffusion is calculated in the same manner.

Electron and ion temperature equations

The equations for the electron and ion temperature are

$$\frac{\partial \theta_e}{\partial t} = \frac{\theta_i - \theta_e}{\tau_{eq}} + \frac{\gamma - 1}{\rho}\left\{ \hat{\eta} j^2 - \hat{P}_{rad} + \nabla . \hat{\kappa}_e \nabla \theta_e \right\} \qquad (4.45)$$

$$\frac{\partial \theta_i}{\partial t} = \frac{\theta_e - \theta_i}{\tau_{eq}} + \frac{\gamma - 1}{\rho}\left\{ \frac{\hat{\mu}}{r^2}\left(\frac{\partial}{\partial r}(rv)\right)^2 + \nabla . \hat{\kappa}_i \nabla \theta_i \right\} \qquad (4.46)$$

These equations are coupled by the equipartition term τ_{eq} . For most of the simulation the timestep is much shorter than the equipartition time, and we can split the solution into two stages: solve the equations separately omitting the equipartition term, and then calculate the effect of the equipartition term. This procedure leads to the solution of two tridiagonal systems of equations and a 2 x 2 matrix inversion at every point. The alternative approach is to difference eqs(4.45),(4.46) as they stand, which leads to a block-tridiagonal system of equations. This can be inverted by an algorithm which is a direct generalisation of the standard tridiagonal inversion routine (Marsh and Potter, 1982), but which is more complex. Both approaches were tried, and the results agreed very well. Since the results agreed, the simpler split method was used for all the runs described in this thesis.

The program conserves mass to better than one part in 10^9 . Because the energy equation is not written in conservative form, energy is only conserved to 1.2% over 200 timesteps in an ideal run. For a non-ideal run, the external energy input is much larger than this change in energy from non-conservation.

The timesplitting scheme used is formally accurate to $O(\Delta t)$ since fully implicit differencing is used for the transport terms.

4.4 Wall current model with resistive diffusion

The sliding rezone program ZPLAG was originally run with the wall current model described in chapter 3. This model does not describe resistive diffusion of flux through the boundary plasma; in this section a more realistic wall current model is derived which does treat this important physical effect.

If we write the magnetic flux as

$$\underline{\Phi} = \int \underline{B} \cdot d\underline{S} \tag{4.47}$$

Using Alfven's theorem (Ferraro and Plumpton, 1966), we can write the rate of change of flux as

$$\frac{d\underline{\Phi}}{dt} = \int \frac{\partial \underline{B}}{\partial t} \cdot d\underline{S} - \oint \underline{v}_b \times \underline{B} \cdot d\underline{l} \tag{4.48}$$

$$= - \oint \underline{E} \cdot d\underline{l} - \oint \underline{v}_b \times \underline{B} \cdot d\underline{l} \tag{4.49}$$

Taking the boundary velocity v_b equal to the fluid velocity at the piston position and equal to zero at the wall, we obtain

$$\frac{d\underline{\Phi}}{dt} = - (v_r B_\theta + \eta j)\Big|_{wall} \tag{4.50}$$

When the plasma is collapsing, $d\underline{\Phi}/dt > 0$ as before, and flux can be driven in as specified by the external circuit. However, as we

require that $v_r \lesssim 0$, we can see that the flux can only decay by resistive diffusion through the wall plasma. Therefore, when the pinch is expanding

$$\frac{d\bar{\Phi}}{dt} = \eta j\big|_{wall} \tag{4.51}$$

We make the assumption that the wall plasma layer carrying the current is several Larmor radii thick, and so we can write

$$j_{wall} = \frac{-\bar{I}_w}{2\pi r_w r_L} \tag{4.52}$$

where r_L is the Larmor radius at the wall.

If we now write $\bar{\Phi}' = -\bar{I}\log r/r_w$, we find that

$$\frac{d\bar{\Phi}'}{dt} = \frac{-\eta \bar{I}_w}{\mu_0 r_w r_L} \tag{4.53}$$

and therefore eq (3.24) becomes

$$\frac{d\bar{I}_w}{dt} = -\frac{(\bar{I}_0+\bar{I}_w)}{r_p \log r_p}\frac{dr_p}{dt} - \frac{\eta \bar{I}_w}{\mu_0 r_w r_L} \tag{4.54}$$

This equation is subject to the constraint that $I_0 > 0$

We can obtain an idea of the timescales involved for the resistive decay by noting that the characteristic time for the wall current to decay is given by

$$\tau = \frac{\mu_0 r_\omega r_L}{\eta} \qquad (4.55)$$

For a wall plasma at a temperature of 1 eV and taking $r_\omega = 10^{-2}$ m, $r_L = 10^{-4}$ m, we find $\tau \simeq 12$ns. This means that resistive diffusion through the wall plasma is an important effect for the particular configuration considered here.

4.5 Results

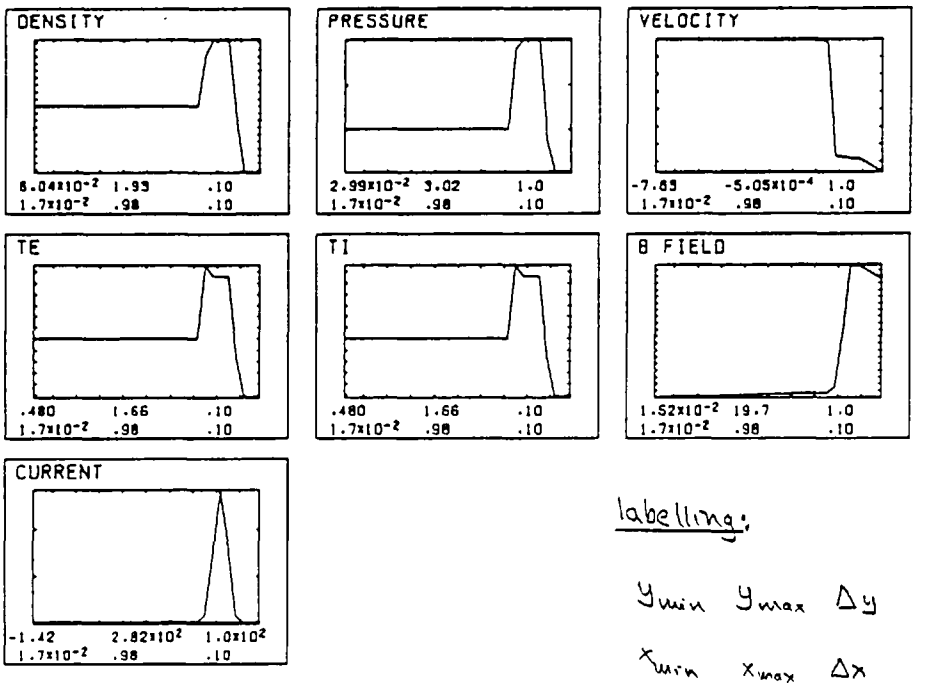
In this section we present results from the Eulerian and sliding rezone programs. Most of the results shown are from the sliding rezone program ZPLAG because these results give better definition in the compressed pinch. However, to illustrate one or two points, some results from the Eulerian program are presented as well.

In figs 4.1 and 4.2 we show the results given by the Eulerian program for an ideal run at 300 mTorr (ie the transport terms were turned off). The points to notice about these graphs are the monotonic resolution of the shock provided by the FCT routines, the sharp current profile and the 1/r dependence of the magnetic field in the vacuum region. Because this run is ideal, the electron and ion temperatures are equal.

In fig 4.3 we show a plot of piston position against time for a run at 80 mTorr filling pressure. At 80 mTorr, the results agree with the model described in chapter 1 (see fig 1.4) and with the experimental

All the graphs of the plasma properties have the same format. The quantities plotted against scaled radius are the dimensionless pressure, density, temperatures, magnetic field and current density. They can be converted to dimensional quantities using eqs (4.6 - 4.9) on p70 after three of the dimensional constants have been chosen. The three constants chosen are the initial radius, density and the temperature scale is chosen so that the plotted temperatures are in eV (see p 75).

TIME= 28.2 NSTEP= 150



labelling:

y_{min} y_{max} Δy

x_{min} x_{max} Δx

Figure 4.1

(see opposite for detailed description of variables)

TIME= 53.7 NSTEP= 750

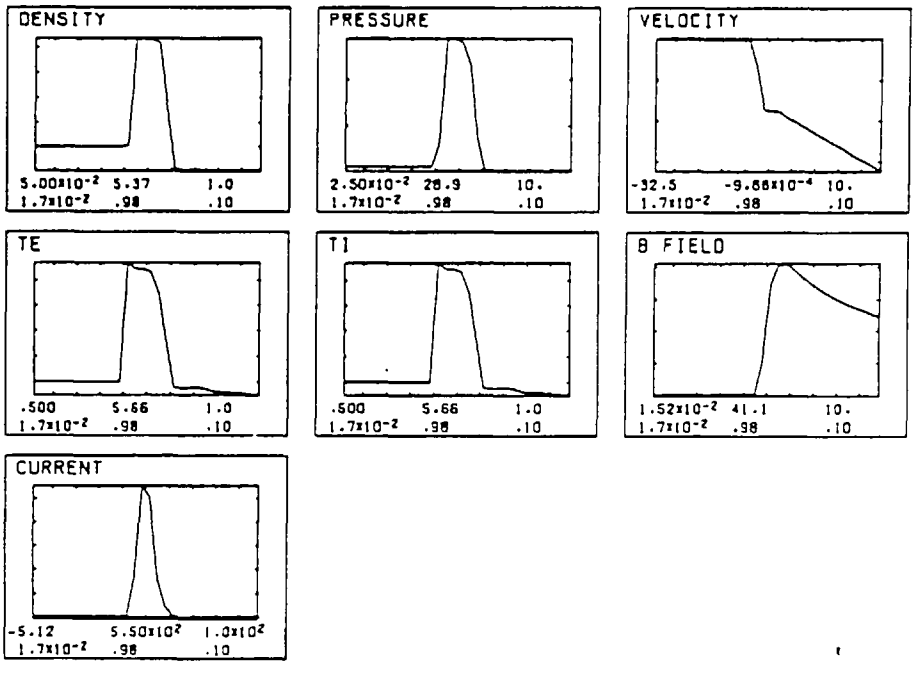


Figure 4.2

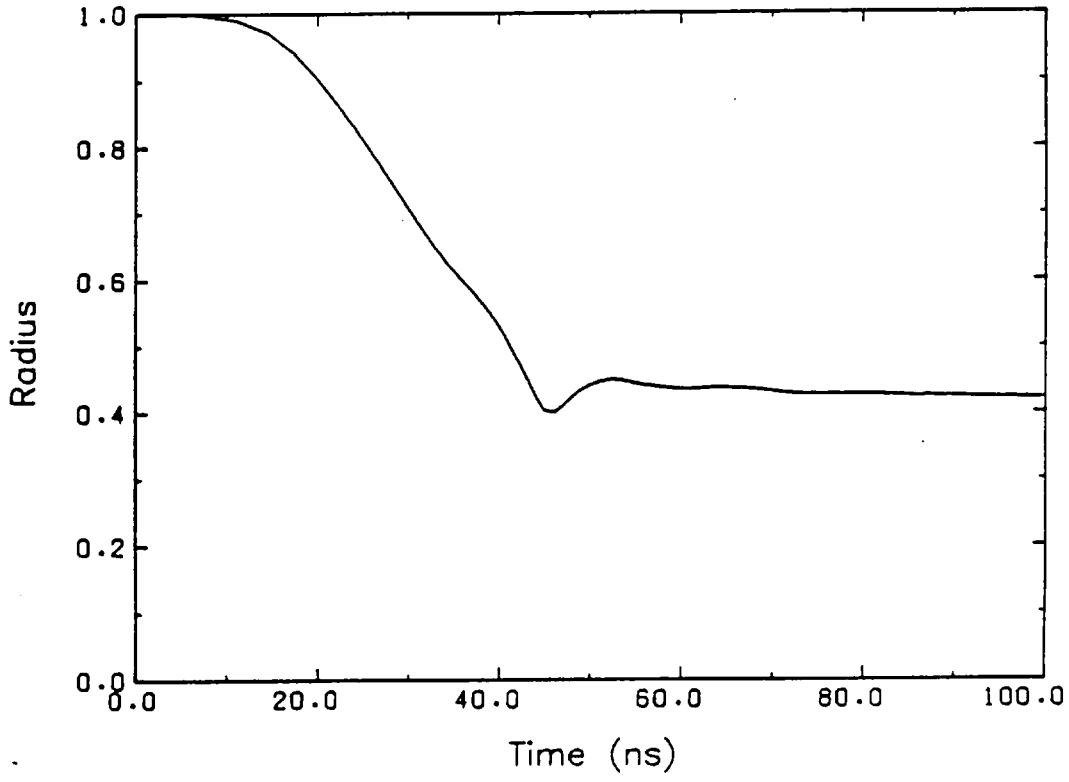


Fig 4.3 Piston position vs time at 80 mTorr with transport terms included

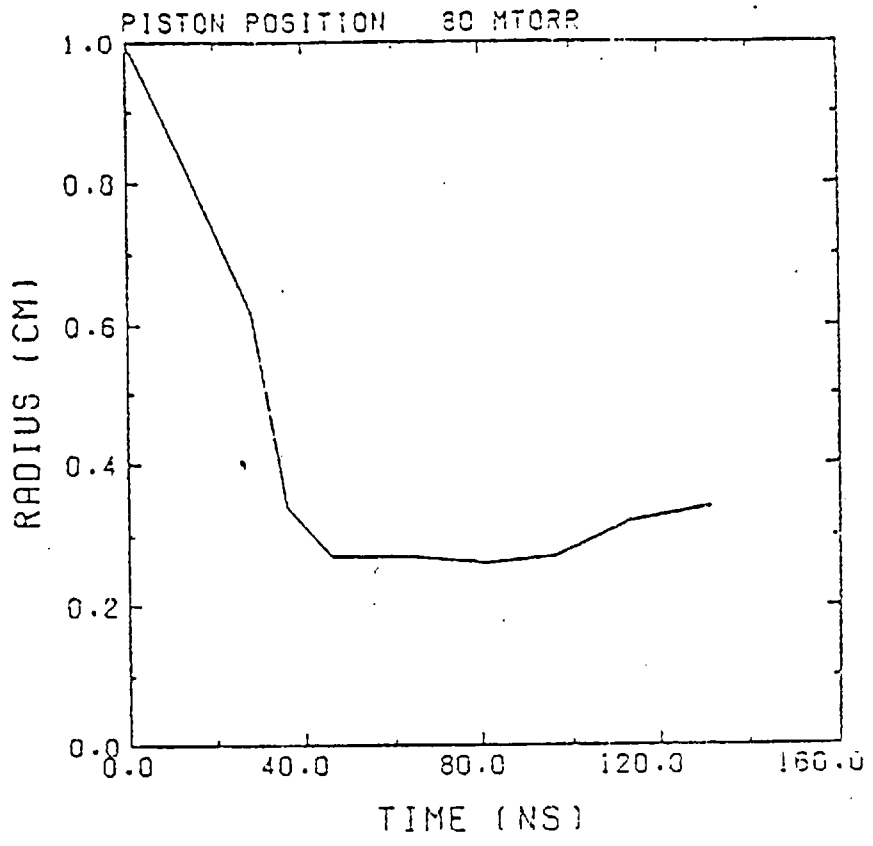


Fig 4.4 Experimental results for a run at 80 mTorr filling pressure

results (see fig 4.4). The purpose of this graph is to show that the model agrees with the previous simulation where the effects of viscosity are important in the final stages of the run. The new results we present are those from a run at 300 mTorr filling pressure. Comparing the results from the calculations described in chapter 1 (see fig1.5) with the experimental trace (fig 4.16), we can see that this regime is clearly not adequately described by Hopkin's model. Further, as we saw in chapter 1, the lack of bounce in fig 4.4 cannot be explained by the slug model either.

The run chosen for illustration models the formation of a 1cm radius pinch with an initial filling pressure of 300 mTorr. The current trace, which is taken from experimental observations, is shown in fig 4.5. For this particular run the initial values used were average values taken from the STARTUP program described in chapter 2. Using the full profiles makes virtually no difference to the solution. The only real differnce occurs when using the Eulerian version ZPEUL, when the higher temperature at the wall causes the plasma to detach from the wall with a sharper density profile. The heat flux limit used was 5%. In their work, Hopkins, Potter and Webb used a heat flux limit of only 1%. Recent experimental work by Wyndham (1982) has observed heat flux limits of about 10% when $T_e \simeq T_i$. For $T_e >> T_i$, Gray et al (1980) observed a heat flux limit of about 4%.

Fig 4.6 shows the profiles of density, pressure, velocity, electron temperature, ion temperature, magnetic field, and current as functions

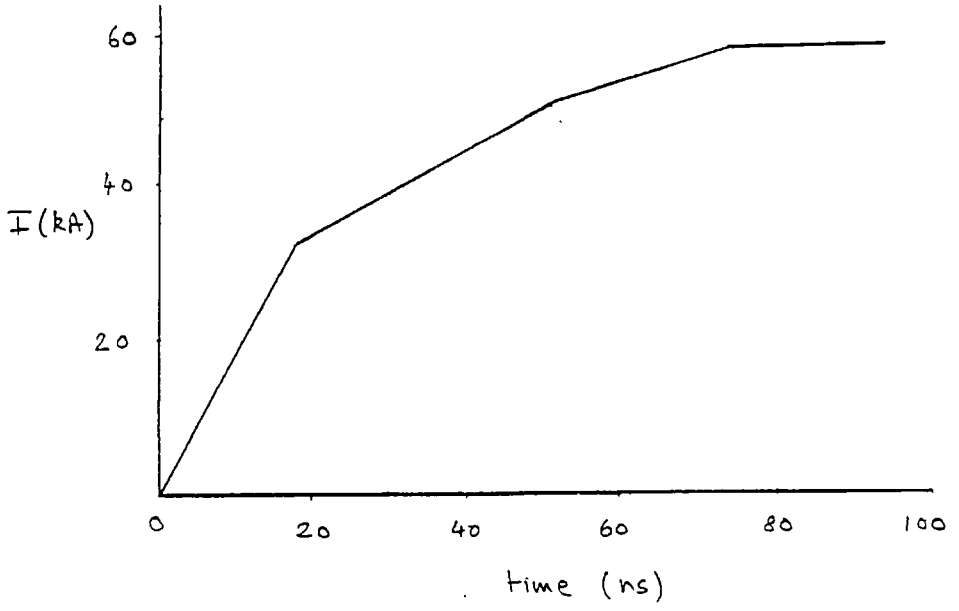


Fig 4.5 Current trace (in kA) as a function of time(ns)

TIME= 51.1 NSTEP= 500

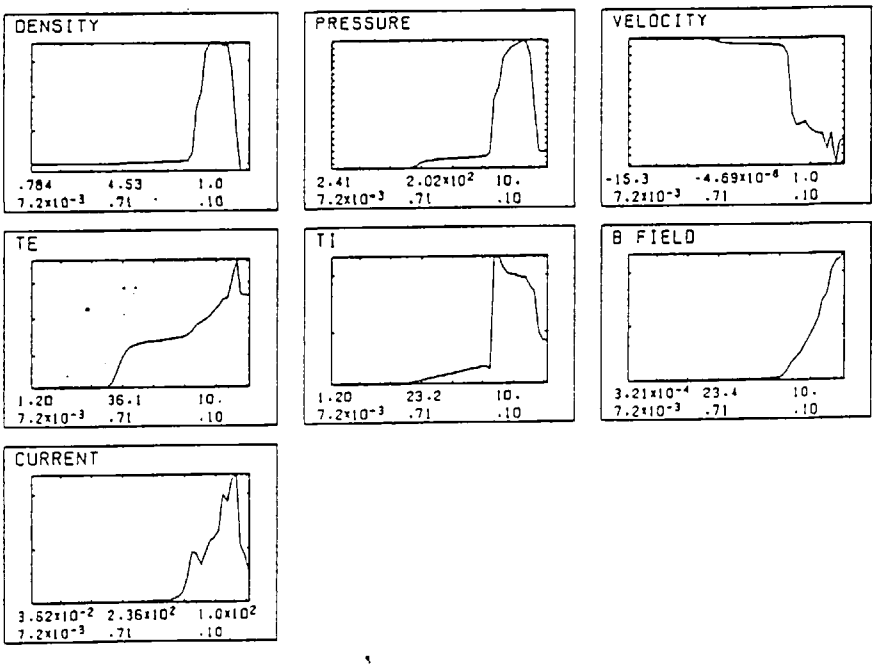


Figure 4.6

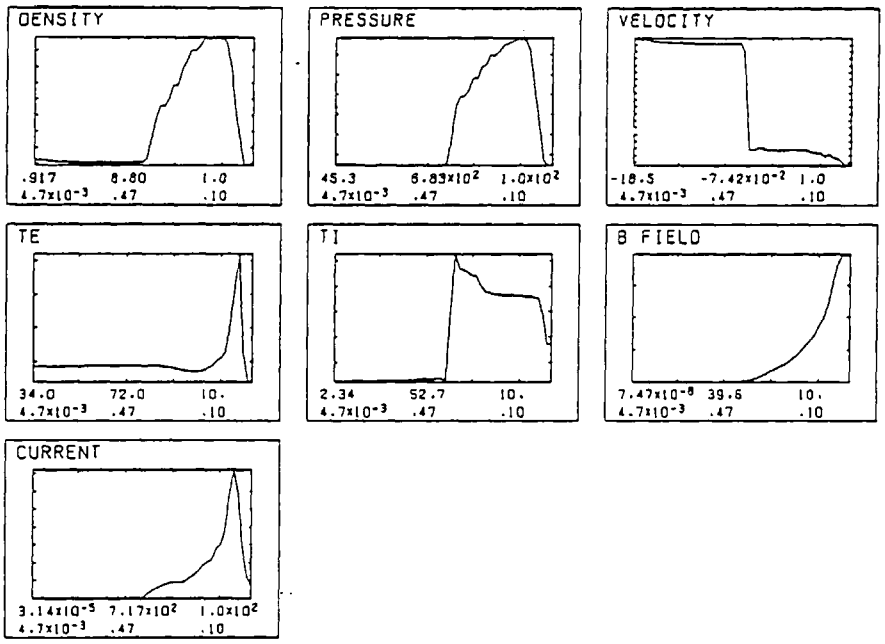


Figure 4.7

TIME= 75.8 NSTEP= 1500

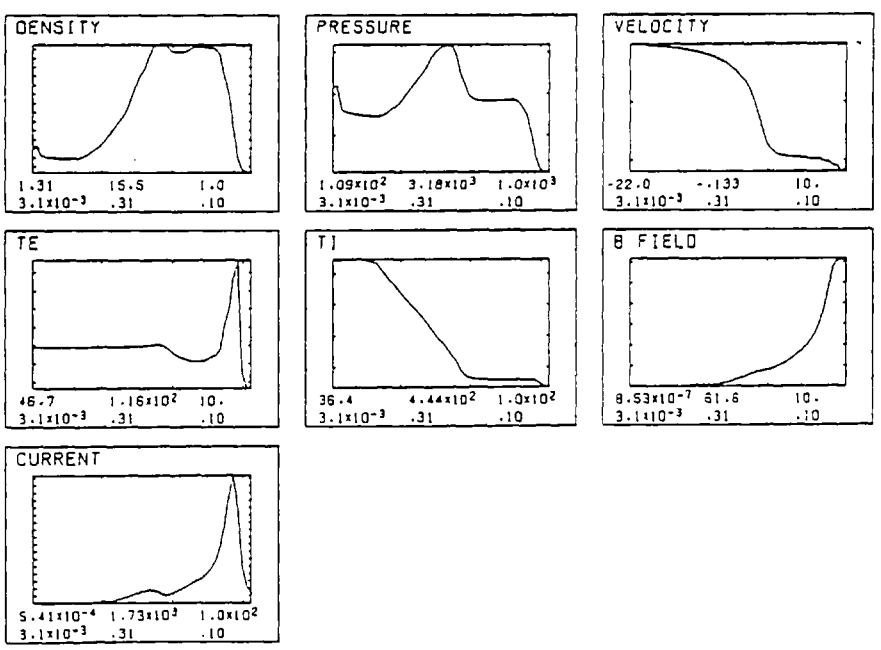


Figure 4.8

of the radius at a time of 51ns. The density jump of 4.5 across the shock agrees reasonably well with the value of 4 predicted by the Rankine-Hugoniot conditions for a steady shock. Exact agreement is not expected because the shock thickness (several Δr) is not small compared with the shock radius ($\Delta r/r \simeq 1/10$). The temperature front in the electron temperature has run on in front of the shock and is preheating the unshocked plasma. Because the ion thermal conductivity is much less than the electron thermal conductivity, the ion temperature front is still coincident with the shock front. There has been some heating of the ions by equipartition and viscous heating. The current has diffused in to about 25% of the pinch radius.

In fig 4.7 the plasma state at 67.7 ns is shown. The pinch boundary is at about 45% of the wall radius, and the pinch is now collapsing quickly. The electron temperature front has reached the axis, but the ion temperature front is still coincident with the shock owing to the smaller ion thermal conductivity.

At 75.8 ns, shown in fig 4.8, the shock has bounced off the axis and is travelling out to the piston. The electron temperature ranges from 70 eV on axis to 116 eV at the edge of the plasma where joule heating is important. The ions have been heated by compression and viscous heating to 440 eV on axis.

Fig 4.9 shows the plasma state at 81 ns. The pinch is now starting to expand with a speed of approximately 25% of the inward speed just

TIME= 81.1 NSTEP= 2000

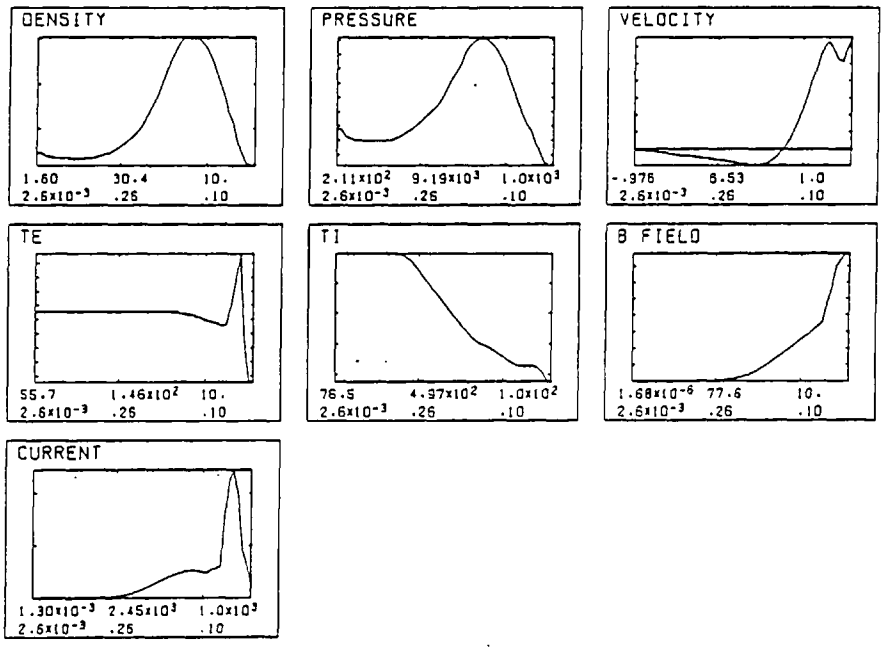


Figure 4.9

TIME= 86.5 NSTEP= 2500

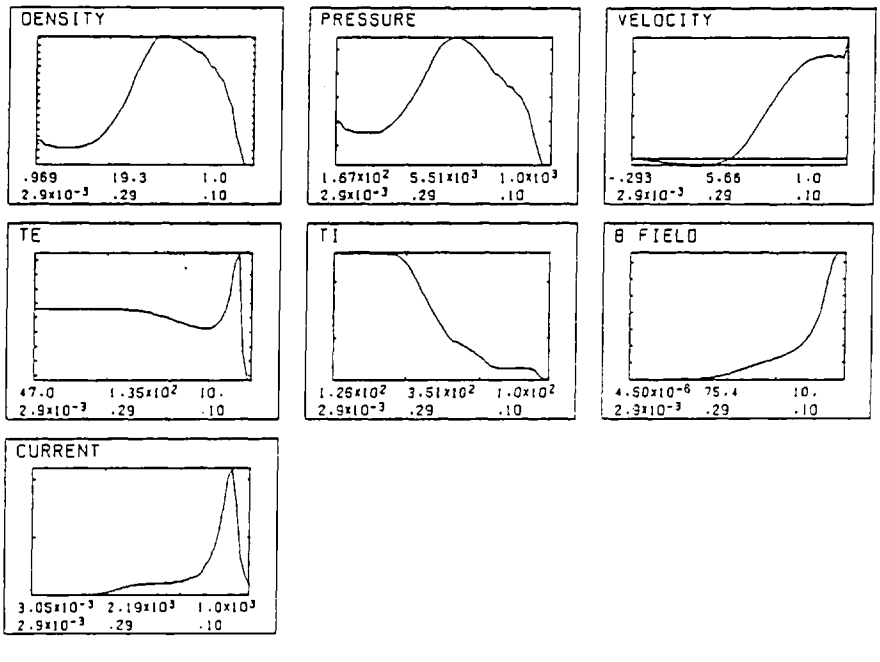


Figure 4.10

TIME= 96.5 NSTEP= 3500

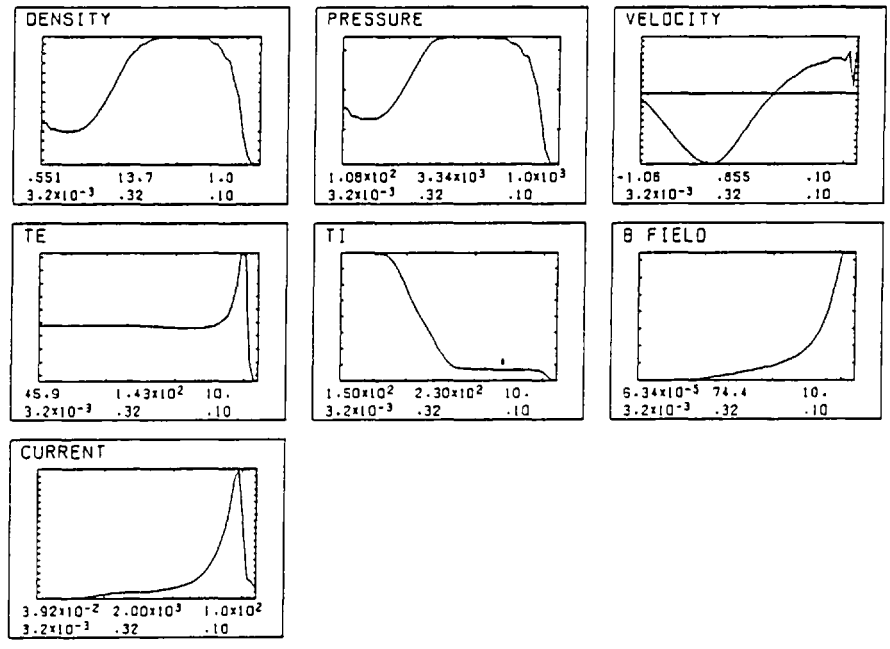


Figure 4.11

TIME= 105.3 NSTEP= 4500

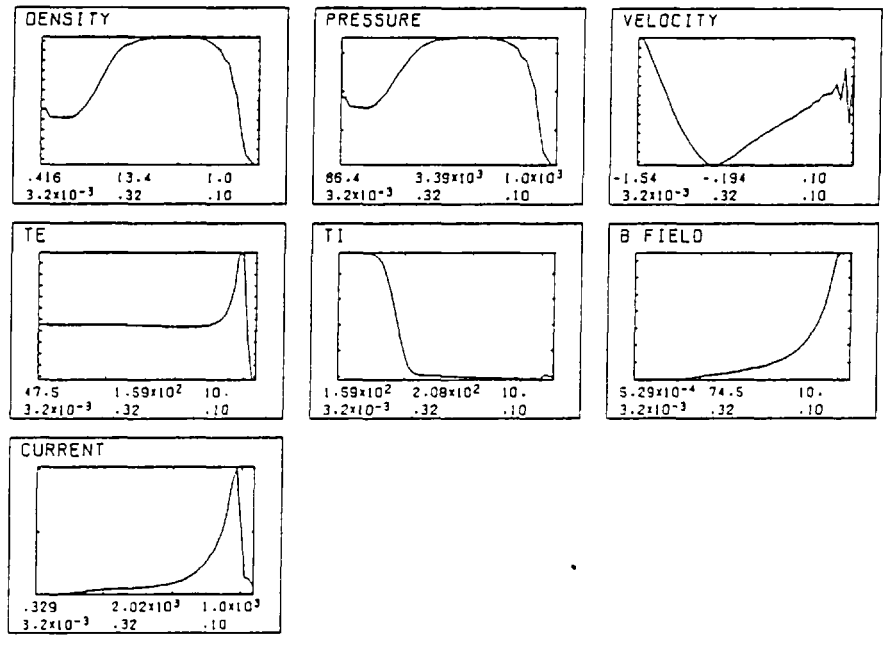


Figure 4.12

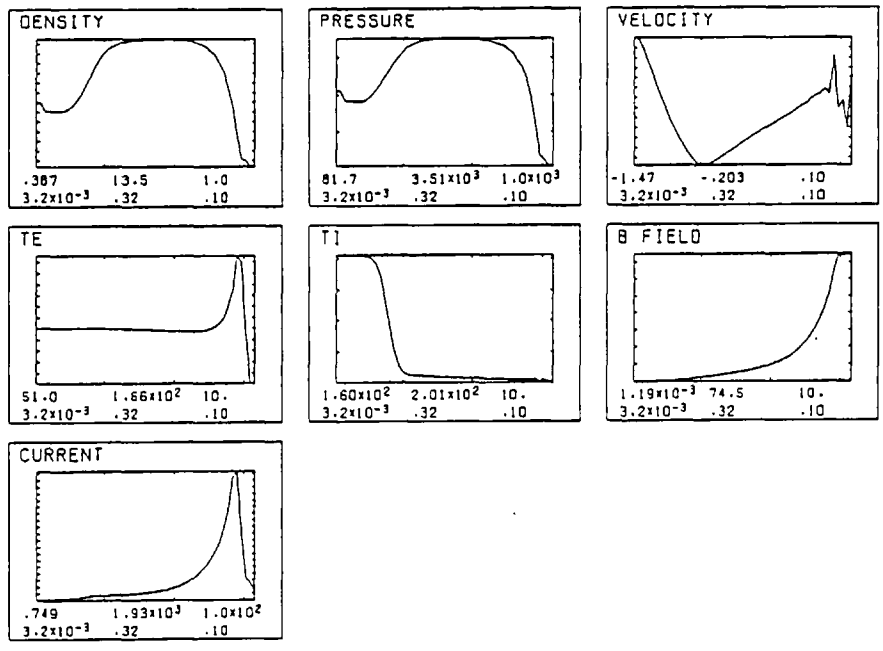


Figure 4.13

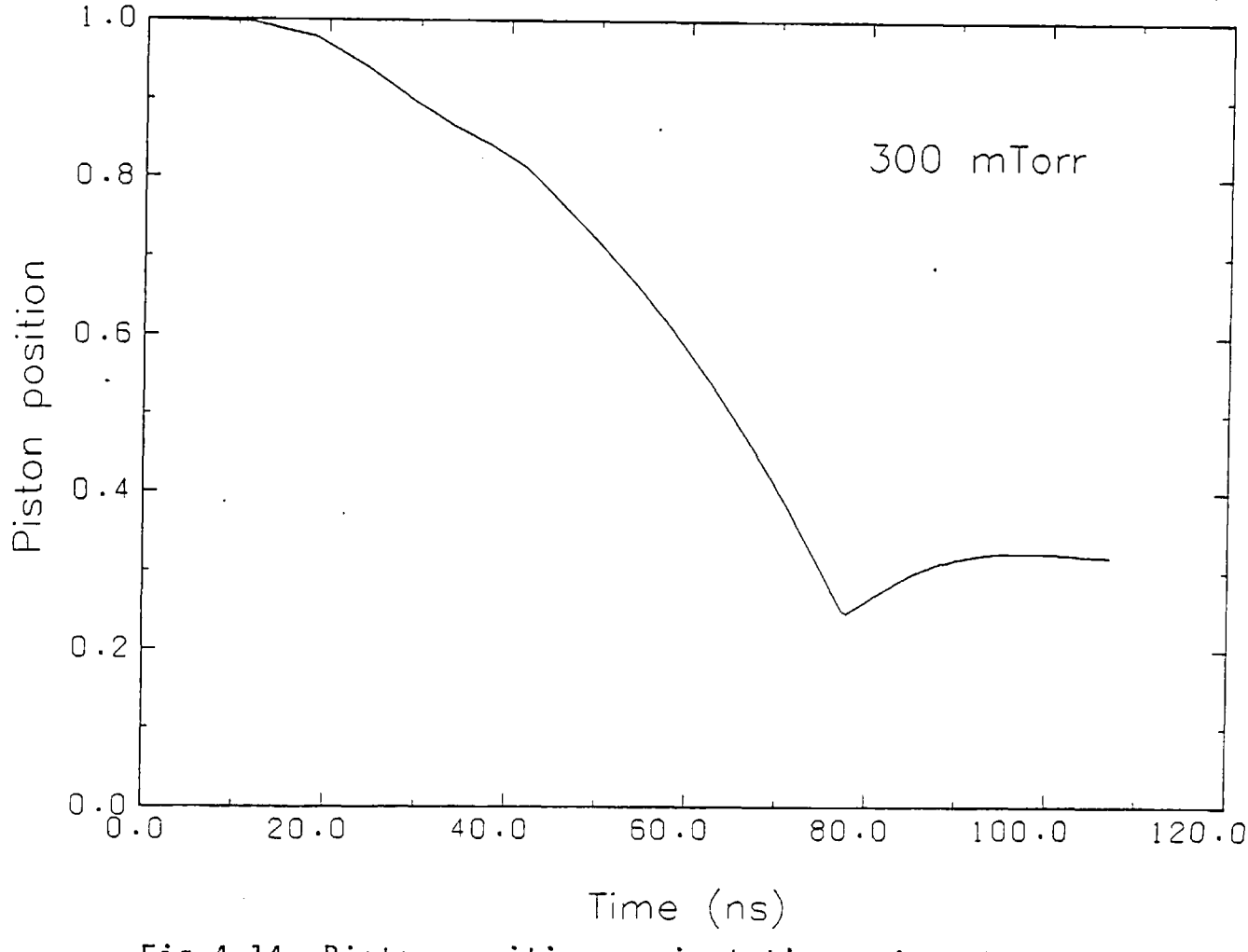


Fig 4.14 Piston position against time using the sliding rezone model

before peak compression. The minimum pinch radius is .26r . The electron temperature is about 100 eV on axis rising to 146 eV at the current sheet where the joule heating is high, and the ion temperature has risen to nearly 500eV on axis.

In fig 4.10 the plasma is shown at 86.5 ns. The plasma is still expanding, but the rate of expansion is decreasing as a result of the wall current. The expansion has caused both the electron and ion temperatures to drop - the electron temperature to just over 90 eV and the ion temperature to 350 eV. In fig 4.11 the pinch boundary is at .32 and the boundary velocity is nearly zero.

Finally, comparing fig 4.12 and 4.13 shows very little variation in the plasma variables over 4 ns. The pinch is nearly in equilibrium, with some fluid motion in the centre of the pinch where nothing balances the radial pressure gradient.

The plot of piston position against time for this run is shown in fig 4.14. For comparison the same plot from the Eulerian program is shown in fig 4.15 and the experimental trace is shown in fig 4.16. The results of including the resistive diffusion of flux through the wall are shown in figs 4.17 and 4.18. Fig 4.17 shows the predicted trace of piston position against time, and fig 4.18 shows the size of the wall current normalised to the pinch current. It can be seen that including the effect of the resistive diffusion of flux through the wall plasma leads to good agreement with the experimental results.

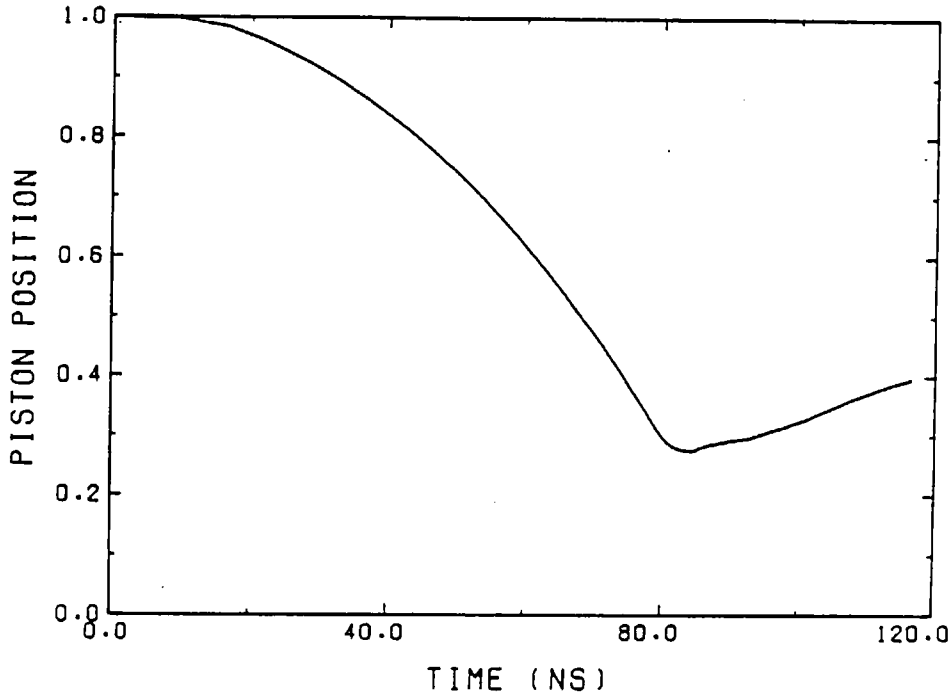


Fig 4.15 Piston position against time using the Eulerian version of the program

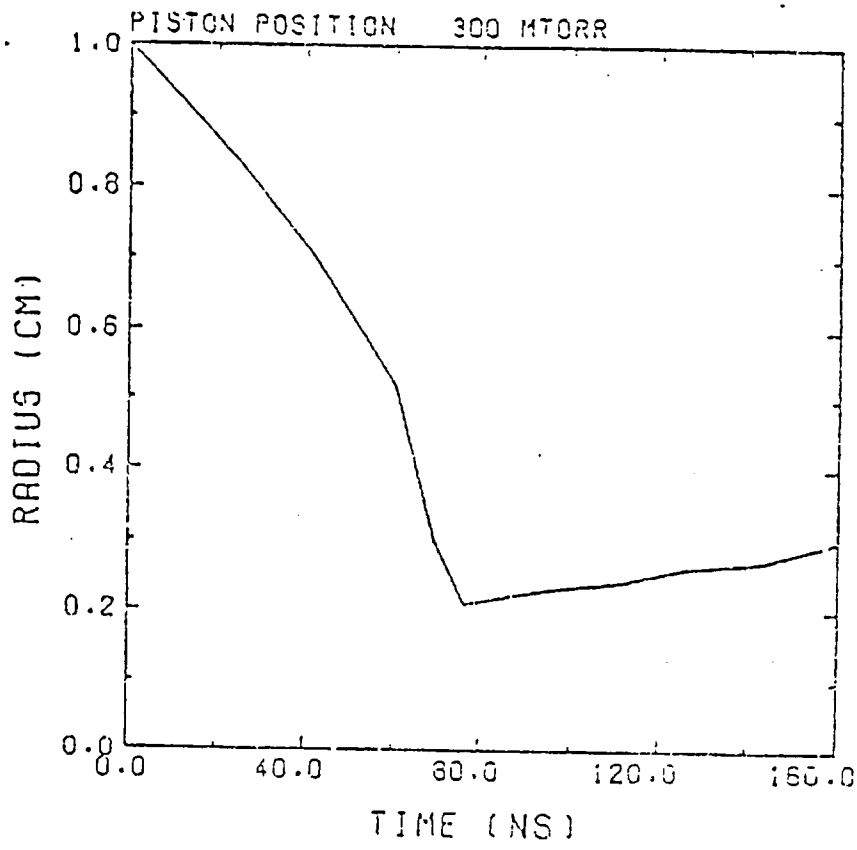


Fig 4.16 Experimental piston position as a function of time (ns)

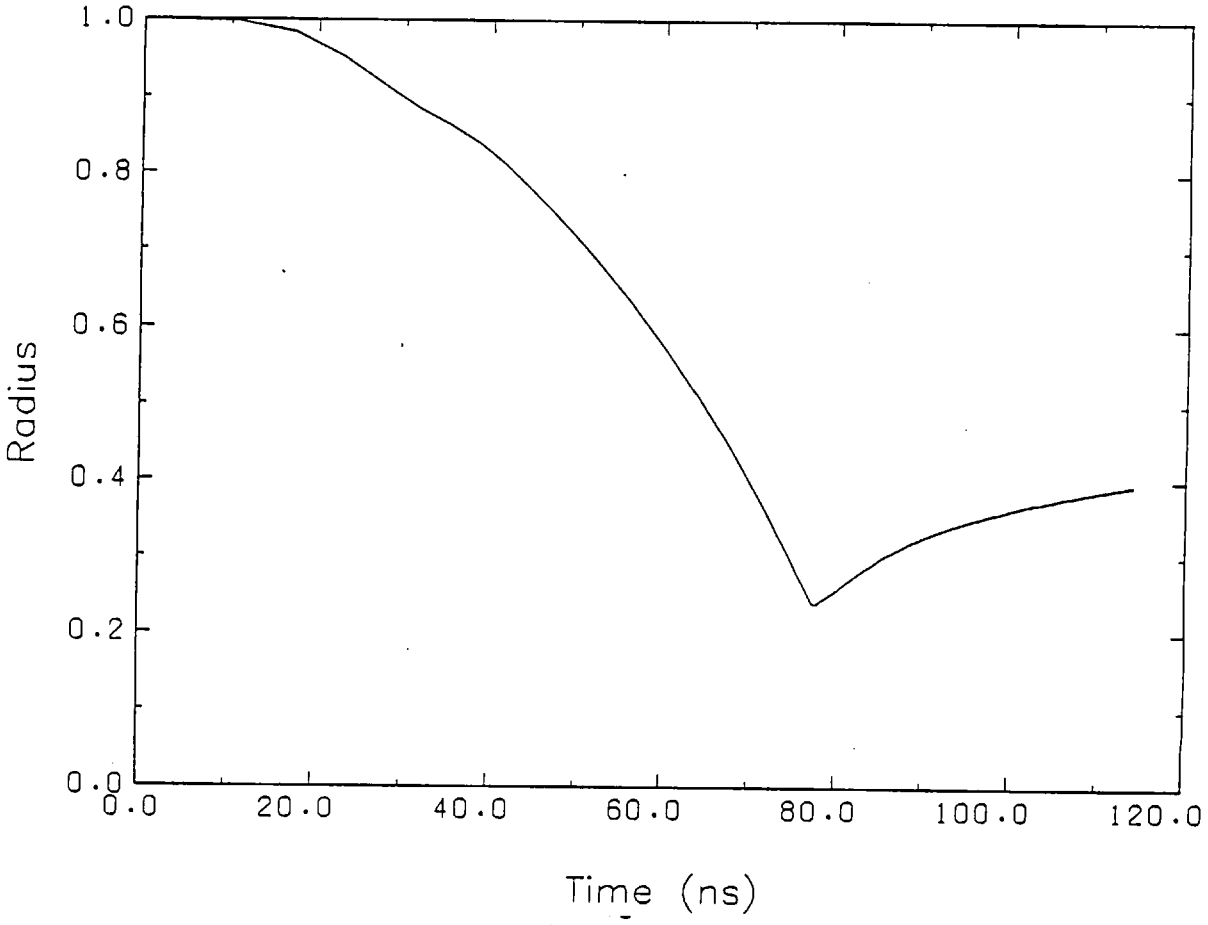


Fig 4.17 Piston position when resistive decay of wall current is included

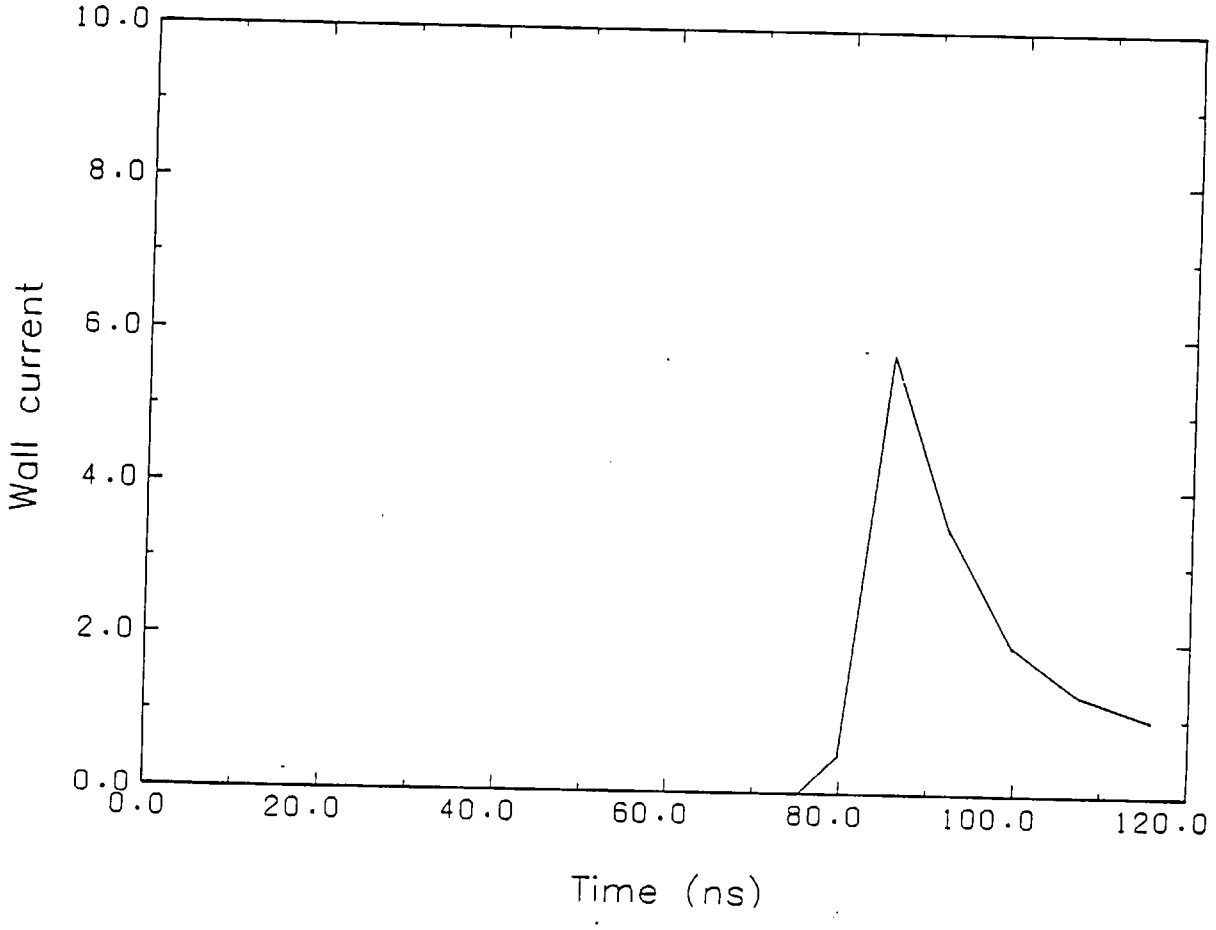


Fig 4.18 I_{wall} / Iext against time in ns

It is worthwile to comment on the results shown in fig 4.15 from the Eulerian program. The reason that the results shown in figs 4.15 and 4.17 agree is a result of the mesh size used for the Eulerian calculation. The decay of the wall current is governed by the Larmor radius at the wall, which determines the thickness of the current sheet. In the Eulerian program the thickness of the current sheet is determined by the mesh size, and for the results shown these values were about the same size.

Comparison of theory (figs 4.14, 4.15, 4.17) with experiment reveals only one major discrepancy - namely that the experimental trace is consistently lower than the theoretical predictions. We can obtain a possible explanation for this if we consider how the trace is calculated.

The experimental trace of piston position is calculated from inductance measurements under the assumption of infinite conductivity. The time integral of the voltage across the pinch is measured, and the inductance is calculated from

$$L(t) = \frac{1}{I(t)} \int V dt \tag{4.56}$$

Using the inductance for a pinch with a sheet current

$$L(t) = \frac{\mu_0}{2\pi} \log r_w / r_p(t) \tag{4.57}$$

the piston radius can be calculated as a function of time.

There are two pertinent comments to be made about this method:

(1) the experimental errors will be greatly increased by taking the exponential to find $r_p(t)$.

(2) no allowance is made for diffusion of current into the plasma.

We cannot do anything about point (1), but we can calculate the likely effect of the diffusion of the current into the plasma. To obtain an idea of the effect let us consider a current distribution defined by:

$$j(r) = 0 \qquad r < \lambda r_p$$

$$= \frac{I}{\pi r_p^2(1-\lambda^2)} \qquad \lambda r_p < r < r_p$$

$$= 0 \qquad r_p < r$$

The inductance is then given by

$$L = \frac{\mu_0}{2\pi}\left(\log r_w/r_p + \frac{1-\lambda}{2(1+\lambda)} \right) \tag{4.58}$$

If we calculate the size of λ by comparing the measured piston position with the predicted piston position, we obtain a value of $\lambda = .2$. Examining fig 4.9 shows this value of λ to be a reasonable estimate of the current diffusion. Making allowance for the effect of current diffusion, we can say that we have achieved excellent agreement between simulation and experiment over a wide range of filling pressures.

One point which needs to be made however is the effect of the strong temperature dependence of the resistive decay of the wall current. This effect depends of the resistivity which varies as $T^{-3/2}$. We have taken T_{wall} to be 1 eV and obtained good agreement with experiment. Changing the wall plasma temperature by a factor of three would change the effect of the wall current by an order of magnitude. It would be very useful to have a more detailed picture of the plasma at the wall so that the temperature of the wall plasma could be calculated; this would substantiate the model completely.

4.6 Conclusions

In this chapter we have described a realistic 1-d two temperature MHD model which simulates the formation of a z-pinch. The program has a flexible modular programming approach and uses the FCT routines of Boris and Book (1973). Two versions of the program were discussed: the first was an Eulerian program using Hain's method to treat the vacuum plasma. An extra condition was imposed to treat the effects of wall currents. This version treated resistive diffusion of magnetic flux through the low density plasma, but did not provide very good resolution of the compressed pinch.

The second version used a sliding rezone grid and the wall current model of chapter 3 to provide good resolution of the compressed pinch, but did not treat the resistive decay of the wall current. A version of the wall current model which allowed resistive decay of the wall

current was derived and implemented in this version of the program. The results then agreed with the Eulerian calculation, while providing good resolution of the compressed pinch.

Results were presented from a run at 300 mTorr filling pressure. At this filling pressure the model described by Hopkins et al (1978) differed substantially from the experimental observations. Using the wall current model excellent agreement was obtained between simulation and experiment. A consistent deviation from theoretical predictions was explained by including the effect of current diffusion in the experimental analysis.

CHAPTER 5

5.1 Introduction

In this chapter we apply the ideas described in chapters 3 and 4 to m = 0 instabilities in a z-pinch. The work as originally planned involved writing a two dimensional program using FCT, which would have been used to investigate the nonlinear evolution of an m = 0 mode in a z-pinch. This work was started, but while it was in progress it was realised that a model used by Book, Ott and Lampe (1976) would provide an answer more efficiently. The model described by Book et al was used to show that even in a favourable configuration the effect of the wall current was small right into the nonlinear development of the instability (Christie, 1982).

In section 5.2 we discuss the 2-D FCT work. The plan here was to use an ideal MHD program with a sheet current and a boundary following routine to investigate the nonlinear evolution of an m = 0 mode with wall currents. An ideal MHD program using timesplit FCT was written and a boundary following algorithm was coded up. The boundary tracking routine used a height function method and as such was rather crude.

In section 5.3 we discuss the shallow water equations used by Book et al (1976) for long wavelength m = 0 modes. The modification to the dimensionless equations to include the wall current effect is

described and results from the program are presented. The results shown compare the solution obtained without wall currents (ie Book's solution) with the solution obtained when wall currents are included. The configuration chosen was a favourable one yet the difference between the two solutions is only of order 4%. It is doubtful whether this difference could have been detected with the 2-D FCT program.

5.2 A 2-D FCT ideal MHD program

In this section a 2-d FCT program is described. The aim of this work was to model the nonlinear evolution of an m = 0 instability under the influence of wall currents. The approach chosen was a timesplit ideal MHD calculation with a boundary following algorithm. This work was not completed because it was realised that the desired results could be obtained far more efficiently using a method given by Book, Ott and Lampe (1976).

The ideal MHD equations used in 2-d were:

$$\frac{\partial \rho}{\partial t} + \frac{1}{r}\frac{\partial}{\partial r}(r\rho v_r) + \frac{\partial \rho v_z}{\partial z} = 0 \tag{5.1}$$

$$\frac{\partial \rho v_r}{\partial t} + \frac{1}{r}\frac{\partial}{\partial r}(r\rho v_r^2) + \frac{\partial}{\partial z}(\rho v_r v_z) = 0 \tag{5.2}$$

$$\frac{\partial \rho v_z}{\partial t} + \frac{1}{r}\frac{\partial}{\partial r}(r\rho v_r v_z) + \frac{\partial}{\partial z}(\rho v_z^2) = 0 \tag{5.3}$$

where F_r is the radial force and F_z is the force in the z direction. The equation of state was

$$p = \left(\frac{p_0}{\rho_0^{\gamma}}\right)\rho^{\gamma} \tag{5.4}$$

These equations were solved in the usual timeplit manner (eg, Brown 1981). The two body forces were calculated as follows:

(1) The boundary is determined by a height function $r_p(z)$.

(2) In the plasma, we assume the current is zero and set

$$F_r = -\partial p/\partial r$$

$$F_z = -\partial p/\partial z$$

(3) In the vacuum region the force is zero.

(4) The force across the boundary is obtained by integrating the divergence of the electromagnetic stress tensor T across a cell

$$\underline{F} = \int \nabla.\underline{\underline{T}}\, d\tau$$

$$= \int \underline{\underline{T}}.d\underline{S}$$

$$\therefore \underline{F} = \left(p - \frac{B^2}{2}\right)\underline{n} \tag{5.5}$$

The force across the boundary was split into r and z components. These forces were then applied to a representative volume across the boundary. Thus for the example shown

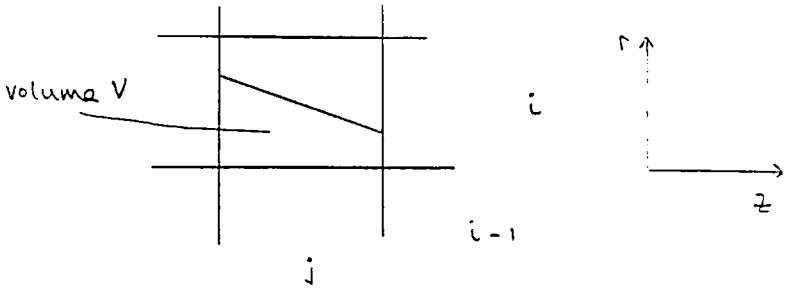


Fig 5.1 Representative finite difference volume

$$F^r_{i,j} = V(p - \beta^2/2)\cos\theta$$

$$F^z_{i,j} = V(p - \beta^2/2)\sin\theta$$

$$f^r_{i-1,j} = -\frac{\partial p}{\partial r}\Big|_{i-1,j} + (1-\nu)(p - \beta^2/2)\cos\theta$$

$$F^z_{i,j-1} = -\frac{\partial p}{\partial z}\Big|_{i,j-1} + (1-\nu)(p - \beta^2/2)\sin\theta$$

The program was left unfinished at this stage. The hydrodynamics had been tested (see fig 5.2), and the boundary following algorithm worked for small movements of the boundary. As the amplitude of the instability grew, the algorithm broke down. This is probably due to the crude boundary tracking algorithm used, particularly as the height function was only specified at the gridpoints z . In view of the shallow water approximation described in the next section, it was not felt worthwile to continue with the program.

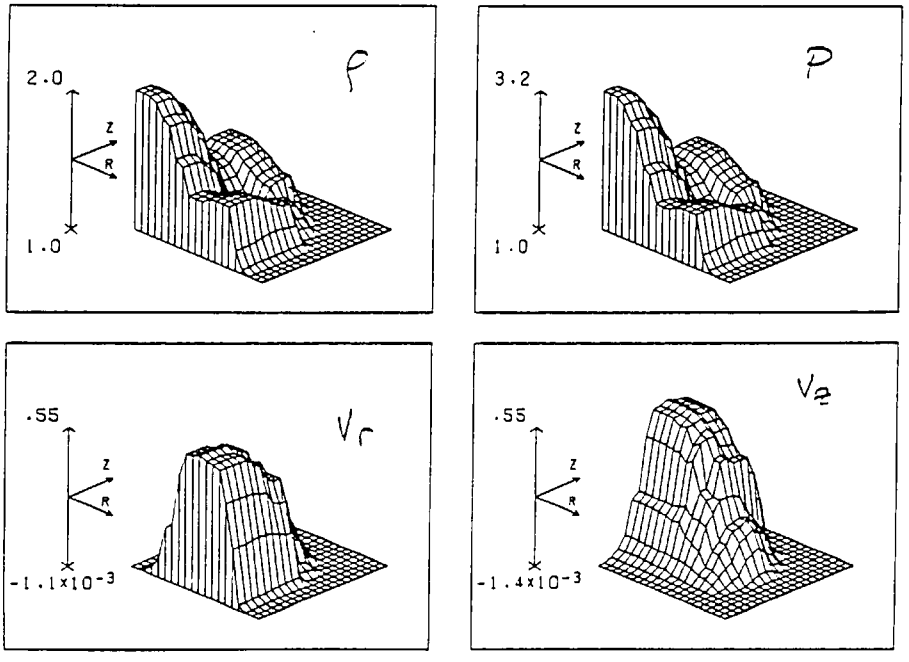


Fig 5.2 Result from 2-d test problem

5.3 The long wavelength limit

In this section we apply the wall current model to a simple model which deals with the long wavelength limit $ka \ll 1$. We expect this limit to be the one in which the wall current model is likely to have the most effect. For short wavelength modes with $ka \gg 1$ the instability will become nonlinear and saturate when the amplitude is still small compared with r. We know from Tayler's work (1957a;1957b) that a combination of a trapped axial field and an infinitely conducting wall can stabilise an m = 0 instability in the z-pinch. It is natural therefore to ask what effect wall currents have on the evolution of an m = 0 instability, and in particular whether they can account for the anomalously long lifetime of the fast z-pinch observed by Choi et al (1978).

The assumptions we make are as follows:

(1) We assume a long wavelength mode with $ka \ll 1$.

(2) We assume an ideal, incompressible uniform density plasma

(3) We assume that the transit time for an Alfven wave to propagate down the length of the tube is small compared with the growth time of the instability.

The last assumption changes the model from that considered by Tayler in that it assumes that the wavelength is short enough for the "vacuum" plasma to be moved around the region. The validity criterion for assumption (3) can be written as $kLc_s \ll v_A$. For the z-pinch experiment considered, this criterion is certainly satisfied.

The numerical model we use is the one used by Book, Ott and Lampe (1976) to investigate the nonlinear evolution of an m = 0 mode in a z-pinch. They assumed an incompressible, perfectly conducting z-pinch with uniform density. They followed the full nonlinear development of an m = 0 instability and found that a "spike and bubble" shape formed.

Taking the assumptions (1) - (3) above the fluid equations become

$$\frac{1}{r}\frac{\partial}{\partial r}ru + \frac{\partial v}{\partial z} = 0 \tag{5.6}$$

$$\rho_0\left(\frac{\partial u}{\partial t} + u\frac{\partial u}{\partial r} + v\frac{\partial u}{\partial z}\right) = -\partial p/\partial r \tag{5.7}$$

$$\rho_0\left(\frac{\partial v}{\partial t} + u\frac{\partial v}{\partial r} + v\frac{\partial v}{\partial z}\right) = -\partial p/\partial z \tag{5.8}$$

with boundary conditions

$$\frac{\partial a}{\partial t} + v\frac{\partial a}{\partial z} = u \tag{5.9}$$

$$p(a,t) = \frac{B^2(a(t))}{2\mu} \tag{5.10}$$

Introducing the wavenumber k and writing the equations in terms of the dimensionless variables $R = r/a_a$, $Z = kz$, $T = \gamma t$, $P = p/p_o$, $A = a/a_o$ $U = u/\gamma a_a$, $V = kv/\gamma$ where $\gamma = k(p_o/\rho_0)^{1/2}$ is the linear growth rate

in the long wavelength limit, the equations become:

$$\frac{\partial V}{\partial z} + \frac{1}{R}\frac{\partial}{\partial R}(Ru) = 0 \tag{5.11}$$

$$\frac{\partial V}{\partial T} + V\frac{\partial V}{\partial z} + u\frac{\partial V}{\partial R} = -\partial P/\partial z \tag{5.12}$$

$$\frac{\partial P}{\partial R} = -\epsilon\left(\frac{\partial u}{\partial T} + V\frac{\partial u}{\partial z} + u\frac{\partial u}{\partial R}\right) \tag{5.13}$$

$$(\epsilon \equiv (ka)^2)$$

with boundary conditions

$$\frac{\partial A}{\partial T} + V\frac{\partial A}{\partial z} = u \tag{5.14}$$

$$P = A^{-2} \tag{5.15}$$

In the limit $\epsilon \to 0$ eq(5.13) shows that P is independent of R. From eq(5.12), if V is initially independent of R it remains so, and eq(5.11) can be solved to show that

$$u = -\frac{1}{2} R \frac{\partial V}{\partial z} \tag{5.16}$$

The resulting equations then give

$$\frac{\partial V}{\partial T} + V\frac{\partial V}{\partial z} = -\partial P/\partial z \tag{5.17}$$

$$\frac{\partial A^2}{\partial T} + \frac{\partial}{\partial z}(A^2 V) = 0 \tag{5.18}$$

$$P = A^{-2} \tag{5.19}$$

The eigenfunctions of the linearised eqs(5.17) - (5.19) representing growing modes are:

$$A^2 = 1 + \delta \cos kz\, e^{kT} \tag{5.20}$$

$$V = -\delta \sin kz\, e^{kT} \tag{5.21}$$

Eq(5.19) comes from assuming constant current in the boundary condition

$$p = \mu_0 I^2 / 8\pi a^2$$

With the constant flux condition, this becomes

$$P = L_0^2 / A^2 L^2 \tag{5.22}$$

where

$$L = \int_0^{z_0} \log (r_w / r(z))\, dz \tag{5.23}$$

and r_w is the wall radius.

In the linear stage of the instability, the radius is given by

$$r(z) = a\left(1 + \tfrac{1}{2}\delta \cos kz\, e^{kT}\right) \tag{5.24}$$

Thus from (5.23), taking $kz_0 = 2\pi$,

$$L = L_0 + L_1 \delta^2 \tag{5.25}$$

where

$$L_0 = z_0 \log r_w/a \tag{5.26}$$

and

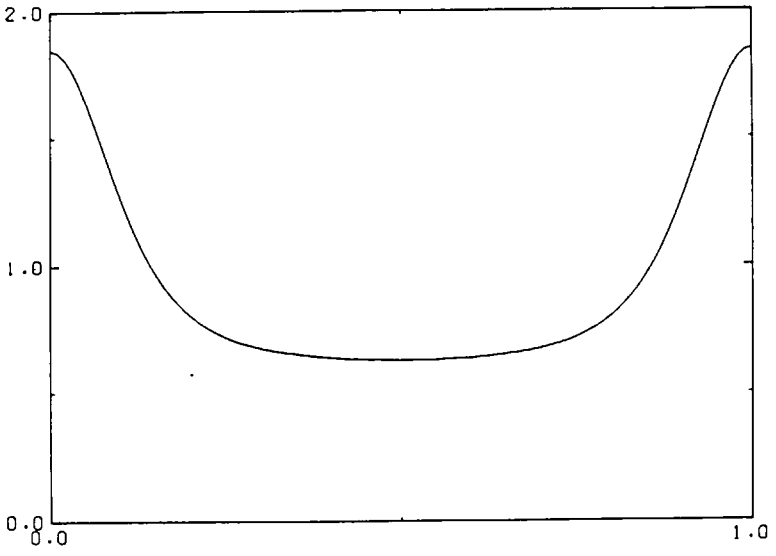
$$L_1 = \frac{e^{2kT}}{8k} \tag{5.27}$$

We see from this that the effect is second order in the amplitude of the perturbation.

Eqs (5.17) - (5.19) were solved by Book et al (1976) using a Lax Wendroff scheme. One problem in solving these equations is that modes with higher wavenumbers have higher growth rates. Thus errors in the solution grow and eventually swamp the desired solution. Book et al found this problem in their work, and were only able to follow the solution for a certain length of time. By using a Lax scheme, which has a higher numerical diffusion for short wavelengths than Lax Wendroff, we were able to follow the solution for a bit longer than with a Lax-Wendroff scheme. The results we obtained agreed with the

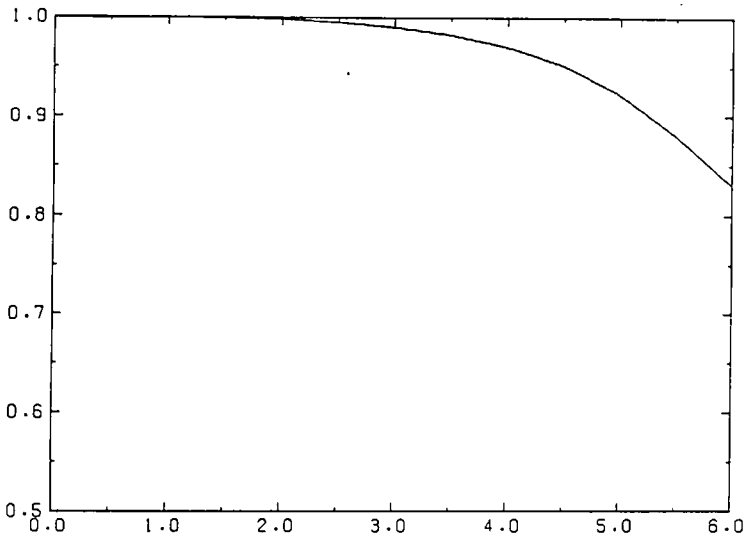
results given by Book et al when eq.(5.19) was used for the pressure. By using eq.(5.22) for the pressure we obtained the effect of the wall currents on the evolution of the instability.

Fig 5.3 shows the nonlinear development of an m = 0 mode with the constant flux constraint. The value of r_o/a chosen was $r_o/a = 2$. In fig 5.4 we show the current normalised to its initial value as a function of the non-dimensional time T. It can be seen that the current only changes in the nonlinear phase of the instability. In fig 5.5, the percentage difference between runs with and without wall currents is shown as a function of Z. The wall current has reduced the amplitude of the perturbation by about 4%.



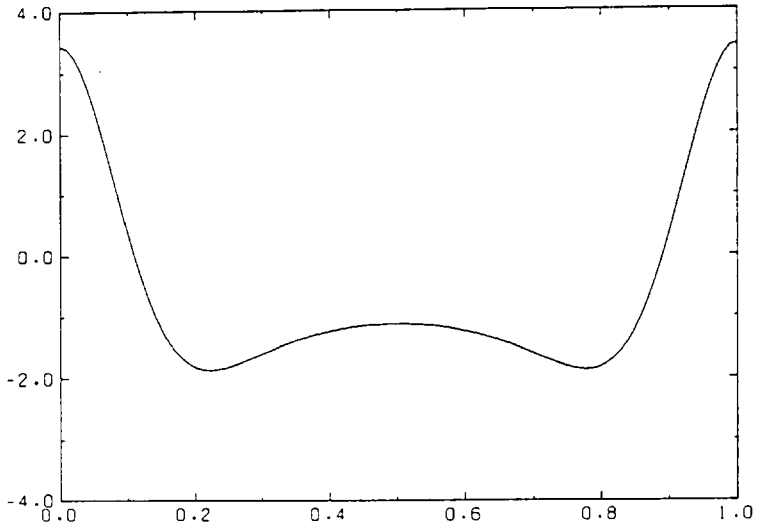
The nonlinear development of an $m = 0$ instability in a Z-pinch at time $T = 6$, with wall currents included.

Figure 5.3



Pinch current I/I_0 as a function for non dimensional time I.

Figure 5.4



Percentage difference between runs with and without wall currents as a function of Z.

Figure 5.5

5.4 Conclusions

In this chapter we have considered the effect of wall currents on the nonlinear evolution of an m = 0 mode in a z-pinch. The first method tried was a 2-d ideal MHD program using Flux Corrected Transport. While this work was in progress it was realised that some work by Book et al (1976) could be adapted to provide the solution more efficiently. The work described by Book et al used a shallow water approximation to study the nonlinear evolution of an m = 0 mode with constant current. Their model was adapted to include the effect of wall currents, and results were presented for a case where a high stabilising effect was expected. Even in the nonlinear stage, the effect of the wall currents was small. We can conclude that the wall current model cannot account for the anomalously long lifetime of the z-pinch observed by Choi et al (1978).

CHAPTER 6

Conclusions

In this work we have been concerned with a practical problem - namely simulating a real z-pinch experiment. We have considered the experiment in the context of analytic models and previous numerical models of pinch formation. Neither the analytic work nor the numerical work gave a complete or satisfactory picture of the formation of the pinch in all regimes. In particular neither approach was able to explain the behaviour of the pinch when viscosity was unimportant.

In chapter 1 we introduced the basic concepts behind the z-pinch experiment. The snowplough and slug analytic models of pinch formation were discussed. Potter's slug model (1978) was described in some detail and an erroneous conclusion was identified. An expression for the pinch boundary as a function of time in a neighbourhood of the pinch time was obtained which predicted a bounce after compression in the same way as the snowplough model and ideal MHD simulations. Finally a previous numerical simulation of the fast z-pinch was discussed. The regions where agreement with experiment was obtained and those where it was not obtained were stated for future reference.

In chapter 2 we examined the preionising phase of the z-pinch using a model given by Killeen, Gibson and Colgate (1960). We started the

calculations with a working gas at room temperature with a seed ionisation fraction of 10^{-6}. The calculations proceeded until we obtained a fully ionised plasma at a temperature of about 1 eV. The results of this chapter were used to provide initial conditions for the programs in chapter 4.

In chapter 3 we discussed methods of modelling z-pinches computationally. The usual method of treating the vacuum region, first given by Hain et al (1960), was described at some length. While it gives the correct physical behaviour during collapse, it does not treat an important physical effect during any subsequent expansion. This effect - trapping of magnetic flux in the low density plasma outside the main pinch - can have an important effect on the pinch expansion after collapse. A simple ideal MHD model in terms of wall currents was presented, and results were given which showed that the effect can inhibit the bounce after compression, and thus bring the simulation closer to experiment. The effect of varying γ - the ratio of specific heats - was discussed briefly: a simple treatment showed that reducing γ would increase the size of the bounce. If a pinch contains impurities and therefore the effective γ is less, the wall currents will be less effective in preventing the bounce.

In chapter 4 we moved on to a detailed MHD simulation of a real experiment. A two temperature MHD model was used and the effects of resistivity, viscosity, electron and ion thermal conductivity and bremsstrahlung radiation loss were included. Rather than modify the

existing program, a new program was written using the Flux Corrected Transport methods of Boris and Book (1973). Two versions of the program exist:

(1) an Eulerian version which models the low density plasma explicitly and

(2) a sliding rezone version using a wall current equation.

The original reason for writing the Eulerian program was that the wall current model of chapter 3 did not treat the resistive diffusion of flux through the wall plasma. Because of the modular structure of the program, changing from one version to the other does not involve a large amount of work. Later on, a more advanced wall current model was included in the sliding rezone program. This resulted in good agreement between the programs, with the more flexible sliding rezone calculation providing better resolution of the pinched plasma. The results from both versions show that the large bounce after compression in runs at high filling pressure is prevented by the wall currents. The slow outward movement of the plasma observed experimentally is shown to be due to the resistive decay of the wall current.

Finally, in chapter 5 we considered the effect of the wall current model on the nonlinear evolution of an $m = 0$ mode. We must consider the nonlinear evolution because the effect is second order in the amplitude of the perturbation. Using a model given by Book, Ott and Lampe (1976), and taking a favourable configuration, we showed that even in the nonlinear stage of the instability the effect is small.

The wall current model has only produced a reduction of about 4% in the amplitude of the mode when the plasma is about to hit the wall.

Artsimovitch L A (1964) Controlled Thermonuclear Reactions Gordon and Breach Science Publishers Inc

Batchelor G K (1970) Introduction to Fluid Dynamics Cambridge University Press

Bateman G (1978) MHD Instabilities MIT press

Beam R M and Warming R F AIAA Journal 16 393

Book D L NRL Plasma Formulary 1980

Book D L, Boris J P, Hain K H J Comp Phys 18 (1975) 243

Book D L, Ott E, Lampe M (1976) Phys Fluids 19 1982

Boris J P NRL Report 2167 1970

Boris J P NRL Memorandum 3273 1976

Boris J P, Book D L J Comp Phys 20 (1976) 397

Boris J P, Book D L (1973) J Comp Phys 11 38

Brown M G (1981) PhD Thesis, University of London

Choi P, Dangor A E, Folkierski A, Kahan E, Potter D E, Slade P D Webb S J (1978)

Proc 7th Int Conf on Plasma Physics and Controlled Thermonuclear Fusion Research IAEA-CN-37-E-3 Vol 2 p69

Christie M A J Phys D: Appl Phys 14 (1981) L73

Christie M A Plasma Phys 24 (1982) 783

Craxton R S (1976) PhD Thesis, University of London

Craxton R S and McCrory R L J Comp Phys 33 (1979) 432

van Dyke M and Guttman A J J Fluid Mech (1982) 120 451

Ferraro V C A and Plumpton C An Introduction to Magnetofluid Dynamics
Clarendon Press, Oxford 1966

Fox L, Mayers D F Computing Methods for Scientists and Engineers
pp 201 - 202 Clarendon Press, Oxford 1968

Gear C W Comm ACM (1971) 14 176

Glimm J Comm Pure Appl Math 18 (1965) 697

Gray D R, Kilkenny J D Plasma Phys (1980) 22 81

Hain K et al Z Naturforsch 15a (1960) 1039

Haines M G (1978) J Phys D: Appl Phys 11 1709

Haines M G (1981) Phil Trans R Soc Lond A 300 649

Hopkins D I J, Potter D E, Webb S J (1978) "One dimensional simulation of a z-pinch", unpublished notes.

Howells P B and Marshall R H in Numerical Methods for Coupled Problems
(1981) Pineridge Press Swansea UK

Killeen J, Gibson G, Colgate S A (1960) Phys Fluids 3 387

Krall N A, Trivelpiece A W Principles of Plasma Physics
McGraw Hill (1973)

Kvartskhava I F et al — Nucl Fusion 11 (1971) 349

Kvartskhava I F et al — (1974) Proc 5th Int Conf on Plasma Physics and Controlled Thermonuclear Fusion Research IAEA-CN-33/E6-6 Vol 3 p149

van Leer B — (1973) Lecture Notes in Physics No 18 163

van Leer B — J Comp Phys 14 (1974) 361

van Leer B — J Comp Phys 23 (1977a) 263

van Leer B — J Comp Phys 23 (1977b) 276

van Leer B — J Comp Phys 32 (1979) 101

Lindemuth I R — J Comp Phys 25 (1977) 104

Marsh F, Potter D E — Comp Phys Commun 24 (1981) 185

Maxon S and Nielsen P D — 1981a UCRL 86151

Maxon S and Nielsen P D — 1981b UCRL 85804

Miyamoto K — Plasma Physics for Nuclear Fusion MIT Press 1980

Mott N F and Massey H S W — Theory of Atomic Collisions p245 2nd edition (1949) Clarendon Press, Oxford

Potter D E — Nucl Fusion 18 (1978) 813

Potter D E	Computational Physics Wiley-Interscience, London (1973)
Roache P J	Computational Fluid Dynamics Hermosa Press, Albuquerque 1972
Rose D T and Clarke M	Plasmas and Controlled Fusion MIT Press, 1965
Roberts K V and Potter D E	Meth in Comp Phys 9 (1970) Academic Press
Sod G A	J Fluid Mech (1976) 83 785
Steger J L and Warming R F	J Comp Phys (1981) 40 263
Tayler R J	Proc Phys Soc B 70 (1957a) 37
Tayler R J	Proc Phys Soc B 70 (1957b) 1049
Wyndham E S	(1982) PhD Thesis, University of London
Zalesak S T	J Comp Phys 31 (1979) 335

APPENDIX

Monotonic Conservative Difference Schemes

High order and low order finite difference schemes each have their own desirable properties. For example a first order scheme such as the Lax scheme or the Courant, Isaacson and Rees scheme (see eg Roache, 1972) has the desirable property of maintaining monotonic solutions near steep gradients. This is achieved only at the expense of smearing out the front over quite a few mesh points. A second order scheme such as Lax-Wendroff provides a steeper front and has less numerical diffusion but has the disadvantage of producing "wiggles" near steep gradients.

In this appendix we will discuss several monotonic conservative difference schemes, including the van Leer schemes and the Flux Corrected Transport schemes. The aim of the monotonic conservative difference schemes is to combine the desirable features of low and high order schemes to provide a finite difference scheme which has only a small numerical diffusion, and yet still provides monotonic profiles near steep gradients.

Random Choice Method

Consider the initial value problem

$$\frac{\partial v}{\partial t} + \frac{\partial f}{\partial x} = 0 \qquad (A.1)$$

with $$v(x,0) = v_L \quad x < 0$$
$$= v_R \quad x > 0$$

This problem is called a Riemann problem. We denote the solution to the Riemann problem by u(x,t).

The RCM is defined by the following algorithm. Writing the finite difference solution as v_i^n then the solution is given by

$$v_i^{n+1} = u(x_i + \theta_i \Delta x, \Delta t) \qquad (A.2)$$

where θ_i is a random variable on the interval (-.5,.5). Glimm (1965) proved that under certain conditions the method will converge to a weak solution of eq(A.1).

Van Leer schemes

Van Leer has published a series of papers entitled "Towards the Ultimate Conservative Difference Scheme" parts I,II,III,IV,V (van Leer 1973, 1974, 1977a, 1977b, 1978). They will be referred to as van Leer I, II, III, IV, V respectively.

In van Leer II, having shown in van Leer I that the Lax-Wendroff

scheme can be made monotonic only at the expense of conservation form, Fromm's zero average phase error scheme (see eg Roache,1972) is made monotonic, and is compared with Godunov's method (see Roache,1972, or van Leer IV). Van Leer uses a slightly different approach from that used in the FCT schemes in that he corrects the solution in terms of the old solution rather than the new solution. The Fromm scheme is made monotonic by adding a third order difference to the Fromm difference operator. The size of the third order difference is controlled by the local smoothness parameter $\Theta = (W_{i+1}-W_i)/(W_i-W_{i-1})$

In van Leer III, the Fromm monotonic scheme is applied to compressible flows. The main result of this paper is that the feedback terms are less effective than had been hoped. In particular, for shock calculations the Fromm monotonic scheme is no longer monotonic and exhibits "wiggles" near steep gradients. Van Leer also finds that the Fromm scheme is far more complicated to program and expensive to run than ordinary second order schemes. This point is of interest for the discussion of the flux vector splitting calculations of Steger and Warming described later in this appendix.

In van Leer IV, upstream weighted schemes based on Godunov's scheme (see eg Roache (1972); for pure convection the Godunov scheme reduces to the Courant, Isaccson and Rees scheme) are presented. Using piecewise approximation in terms of Legendre polynomials, van Leer derives a second order upstream scheme based on the Godunov approach. He makes the scheme monotonic using the methods described in van Leer

II, III. Van Leer's conclusions on the upstream schemes are as follows:

(1) upstream schemes seem natural for numerical convection

(2) upstream schemes can be more accurate than centred schemes

(3) a disturbance does not propagate against the flow

(4) the exact boundary conditions may be specified

Flux Corrected Transport

THe FCT algorithm was first published as SHASTA (SHarp And Smooth Transport Algorithm) by Boris and Book (1973). It has been improved over the years (Book, Boris and Hain, 1975; Boris and Book, 1976; Zalesak, 1979) and a FORTRAN listing of the subroutines in modular form is available (Boris, 1976). Zalesak has given a two dimensional non-timesplit version of FCT (Zalesak, 1979), and has provided a particularly clear explanation of the way that FCT works. He considers the system

$$\frac{\partial w}{\partial t} + \frac{\partial f}{\partial x} = 0 \qquad \text{(A.3)}$$

The high and low order finite difference fluxes are F^H and F^L. The FCT algorithm is given by six steps:

(1) calculate low order fluxes $F^L_{i+1/2}$ (A.4)

(2) calculate high order fluxes $F^H_{i+1/2}$ (A.5)

(3) calculate antidiffusive fluxes:

$$A_{i+1/2} = F^H_{i+1/2} - F^L_{i+1/2} \qquad (A.6)$$

(4) calculate low order solution

$$w^{td}_i = w^n_i - \left(F^L_{i+1/2} - F^L_{i-1/2}\right)\Delta t/\Delta x \qquad (A.7)$$

(5) calculate flux limit $A^C_{i+1/2} = A_{i+1/2}\, C_{i+1/2}$ (A.8)

(6) calculate new solution

$$w^{n+1}_i = w^{td}_i - \left(A^C_{i+1/2} - A^C_{i-1/2}\right)\Delta t/\Delta x \qquad (A.9)$$

The essential step is step (5), the flux limiting stage. The original Boris and Book flux limiter was given by

$$A^C_{i+1/2} = S_{i+1/2}\max\{0, \min[|A_{i+1/2}|, S_{i+1/2}(w^{td}_{i+2} - w^{td}_{i+1})\tfrac{\Delta x}{\Delta t}, S_{i-1/2}(w^{td}_i - w^{td}_{i-1})\Delta x/\Delta t]\} \qquad (A.10)$$

and was inherently one dimensional. Zalesak's flux limiter generalises naturally to multidimensional use.

Steger and Warming's Flux Vector Splitting

Recently Steger and Warming (1982) have published an interesting finite difference scheme for inviscid gasdynamics based on a splitting

of the flux vectors corresponding to positive or negative eigenvalues. An appropriate upstream or downstream weighted difference operator is then used for each split vector. One sided schemes have several useful properties: they usually have better dispersive and dissipative properties than centred schemes and they can have twice the stability bound of a centred scheme (Beam and Warming,1976) and they preserve the sign of positive definite quantities (Roache,1972,p69).

Van Leer has shown that conventional approaches to higher order upwind schemes compare unfavourably with centred schemes in terms of computational efficiency . By splitting the flux vector in such a way that each subvector is associated with eigenvalues of a particular sign,Steger and Warming have removed the upstream/downstream weighting choice from the difference scheme. This results in a scheme which is more robust and computationally efficient than centred schemes. The scheme can be described briefly as follows: The inviscid gasdynamics equations can be written in the form

$$\frac{\partial U}{\partial t} + A(u)\frac{\partial U}{\partial x} = 0 \qquad \text{(A.11)}$$

where $A(u) = \frac{\partial F}{\partial u}$ is the Jacobian matrix and U and F(U) are given by

$$U = \begin{bmatrix} \rho \\ m \\ e \end{bmatrix} \qquad F(U) = \begin{bmatrix} mu \\ mu^2/\rho + p \\ (e+p)u/\rho \end{bmatrix} \qquad \text{(A.12)}$$

The matrix A is give by

$$A = \begin{bmatrix} 0 & 1 & 0 \\ (\gamma-3)u^2/2 & (3-\gamma)u & \gamma-1 \\ (\gamma-1)u^3 - \gamma p u/\rho & \gamma e/\rho - 3(\gamma-1)u^2/2 & \gamma u \end{bmatrix} \qquad (A.13)$$

and its eigenvalues are

$$\lambda_1 = u \qquad \lambda_2 = u-c \qquad \lambda_3 = u-c \qquad (A.14)$$

For locally subsonic flow the eigenvalues are of mixed sign.

Since the system of equations is hyperbolic there exists a similarity transformation Q such that

$$Q^{-1}AQ = \Lambda = \begin{bmatrix} \lambda_1 & & \\ & \lambda_2 & \\ & & \lambda_3 \end{bmatrix} \qquad (A.15)$$

where Λ is a real diagonal matrix

We split Λ into two diagonal submatrices.

$$\Lambda = \Lambda^+ + \Lambda^-$$

where

$$\lambda_i^+ = \frac{\lambda_i + |\lambda_i|}{2} \qquad \lambda_i^- = \frac{\lambda_i - |\lambda_i|}{2}$$

Since the flux vectors are homogeneous of degree 1, Eulers theorem states that F(U) = A.U The splitting is therefore chosen as

$$F^{+} = Q\Lambda^{+}Q^{-1}u$$

$$F^{-} = Q\Lambda^{-}Q^{-1}u$$

and the difference scheme is given by

$$u_j^{n+1} = u_j^{n} - \frac{\Delta t}{\Delta x}\left(\nabla_x F_j^{+} + \Delta_x F_j^{-} \right) \qquad \text{(A.16)}$$

where ∇_x is a backward difference operator and Δ_x is a forward difference operator of the required order. Using simple first order upstream and downstream weighting gives a scheme which is a conservative implementation of the Courant, Isaacson and Rees scheme.

Recently Garlick (1982, private communication) has been using the second order scheme given by Steger and Warming (1982) for calculations of shockwaves propagating outwards from supernova explosions into the interstellar gas. He reports that this method works particularly well on keeping the density and pressure in front of the shock positive, and he also finds that the scheme is just as accurate as FCT and is computationally more efficient.